The Astrophysical Journal, 642:188–215, 2006 May 1

THE EVOLUTION OF THE STAR FORMATION ACTIVITY IN GALAXIES AND ITS DEPENDENCE ON ENVIRONMENT[1]

Bianca M. Poggianti,[2] Anja von der Linden,[3] Gabriella De Lucia,[3] Vandana Desai,[4] Luc Simard,[5] Claire Halliday,[6] Alfonso Aragón-Salamanca,[7] Richard Bower,[8] Jesus Varela,[2] Philip Best,[9] Douglas I. Clowe,[10] Julianne Dalcanton,[4] Pascale Jablonka,[11] Bo Milvang-Jensen,[12] Roser Pello,[13] Gregory Rudnick,[10] Roberto Saglia,[12] Simon D. M. White,[4] and Dennis Zaritsky[10]

Received 2005 October 6; accepted 2005 December 16

ABSTRACT

We study how the proportion of star-forming galaxies evolves between $z = 0.8$ and 0 as a function of galaxy environment, using the O II line in emission as a signature of ongoing star formation. Our high-z data set comprises 16 clusters, 10 groups, and another 250 galaxies in poorer groups and the field at $z = 0.4-0.8$ from the ESO Distant Cluster Survey, plus another 9 massive clusters at similar redshifts. As a local comparison, we use galaxy systems selected from the Sloan Digital Sky Survey (SDSS) at $0.04 < z < 0.08$. At high z most systems follow a broad anticorrelation between the fraction of star-forming galaxies and the system velocity dispersion. At face value, this suggests that at $z = 0.4-0.8$ the mass of the system largely determines the proportion of galaxies with ongoing star formation. At these redshifts the strength of star formation (as measured by the O II equivalent width) in star-forming galaxies is also found to vary systematically with environment. SDSS clusters have much lower fractions of star-forming galaxies than clusters at $z = 0.4-0.8$ and, in contrast with the distant clusters, show a plateau for velocity dispersions ≥ 550 km s^{-1}, where the fraction of galaxies with O II emission does not vary systematically with velocity dispersion. We quantify the evolution of the proportion of star-forming galaxies as a function of the system velocity dispersion and find that it is strongest in intermediate-mass systems ($\sigma \sim 500-600$ km s^{-1} at $z = 0$). To understand the origin of the observed trends, we use the Press-Schechter formalism and the Millennium Simulation and show that galaxy star formation histories may be closely related to the growth history of clusters and groups. If the scenario we propose is roughly correct, the link between galaxy properties and environment is extremely simple to predict purely from a knowledge of the growth of dark matter structures.

Subject headings: cosmology: observations — galaxies: clusters: general — galaxies: evolution — galaxies: fundamental parameters — galaxies: stellar content

Online material: color figures

1. INTRODUCTION

The universe as a whole was more actively forming stars in the past than today (Lilly et al. 1996; Madau et al. 1998; Hopkins 2004; Schiminovich et al. 2005). Studies of galaxies in clusters, groups, and the general field indicate an increased star formation activity at higher redshifts, in all environments. However, a complete mapping of the average star formation activity with redshift as a function of environment has still not been achieved.

A large number of studies, during the last 30 years, have shown that distant clusters generally contain many star-forming galaxies. In fact, the first evidence for galaxy evolution in clusters, and for galaxy evolution in general, has been the detection of evolution in the star formation activity of cluster galaxies, as revealed by photometry and spectroscopy.

Historically, the higher incidence of star-forming galaxies in distant clusters compared to nearby clusters was first discovered by photometric studies of the proportion of blue galaxies, the so-called Butcher-Oemler effect (Butcher & Oemler 1978, 1984; Smail et al. 1998; Margoniner & de Carvalho 2000; Ellingson et al. 2001; Kodama & Bower 2001; Margoniner et al. 2001).

In agreement with the photometric results, spectroscopic studies of distant clusters have found significant populations of emission-line galaxies (Dressler & Gunn 1982, 1983, 1992; Couch & Sharples 1987; Dressler et al. 1999; Fisher et al. 1998;

[1] Based on observations obtained at the ESO Very Large Telescope (VLT) as part of the Large program 166.A-0162 (the ESO Distant Cluster Survey). Based on observations made with the NASA/ESA *Hubble Space Telescope*, obtained at the Space Telescope Science Institute, which is operated by the Association of Universities for Research in Astronomy, Inc., under NASA contract NAS 5-26555. These observations are associated with proposal 9476.

[2] INAF–Osservatorio Astronomico di Padova, Vicolo dell'Osservatorio 5, Padova I-35122, Italy.

[3] Max-Planck-Institut fur Astrophysik, Karl-Schwarzschild-Strasse 1, Postfach 1317, Garching D-85741, Germany.

[4] Astronomy Department, University of Washington, Box 351580, Seattle, WA 98195.

[5] Herzberg Institute of Astrophysics, National Research Council of Canada, 5071 West Saanich Road, Victoria, BC V9E 2E7, Canada.

[6] Institut für Astrophysik, Friedrich-Hund-Platz 1, Göttingen D-37077, Germany.

[7] School of Physics and Astrophysics, University of Nottingham, University Park, Nottingham NG7 2RD, UK.

[8] Department of Physics, University of Durham, South Road, DH1 3LE Durham, UK.

[9] Institute for Astronomy, Royal Observatory Edinburgh, Blackford Hill, Edinburgh EH9 3HJ, UK.

[10] Steward Observatory, University of Arizona, 933 North Cherry Avenue, Tucson, AZ 85721.

[11] Observatoire de Genève, Laboratoire d'Astrophysique Ecole Polytechnique Federale de Lausanne (EPFL), CH-1290 Sauverny, Switzerland. On leave from GEPI, CNRS-UMR8111, Observatoire de Paris, Section de Meudon, 5 Place Jules Janssen, F-92195 Meudon Cedex, France.

[12] Max-Planck-Institut fur extraterrestrische Physik, Giessenbachstrasse Postfach 1312, Garching D-85748, Germany.

[13] Laboratoire d'Astrophysique, UMR 5572, Observatoire Midi-Pyrenees, 14 Avenue Edouard Belin, Toulouse F-31400, France.

Postman et al. 1998, 2001; Balogh et al. 1997, 1998; Poggianti et al. 1999; Tran et al. 2005; Demarco et al. 2005; Moran et al. 2005, to name a few). In contrast, nearby rich clusters (such as Coma) generally are "known" to have relatively few emission-line galaxies. Increased star formation activity in distant clusters is also indicated by the emission properties of composite cluster-integrated spectra (Dressler et al. 2004). In parallel to the cluster studies, the fraction of star-forming galaxies has been found to be higher at $z = 0.3-0.5$ than at $z = 0$ also in groups (Allington-Smith et al. 1993; Wilman et al. 2005b).

While these observations have qualitatively shown that star-forming galaxies were more common in the past than today, quantifying this evolution has proved to be very hard. At any given redshift, the properties of cluster galaxies display a large cluster-to-cluster variance. Disentangling cosmic evolution from cluster-to-cluster variations in a quantitative fashion has not been possible to date due to the relatively small samples of clusters studied in detail at different redshifts. This difficulty in measuring how the fraction of star-forming galaxies evolves with redshift as a function of the cluster properties has affected all types of studies, photometric and spectroscopic, both those based on the O II line from spectroscopic multislit surveys and Hα cluster-wide studies (Couch et al. 2001; Finn et al. 2004, 2005; Kodama et al. 2004; Umeda et al. 2004; Homeier et al. 2005). This might be the reason why a quantitative detection of a clear evolution with redshift in the fraction of star-forming galaxies has been elusive so far (Nakata et al. 2005).

Knowing how galaxy properties depend on cluster and group properties at different redshifts is therefore a necessary condition to assess the amount of evolution with redshift, even before attempting to shed some light on how this evolution depends on environment. General trends were soon discovered by the early studies of nearby clusters, such as the fact that richer, more centrally concentrated, relaxed clusters tend to have proportionally fewer star-forming galaxies than less rich, irregular, unrelaxed clusters. However, an exact portrait of how the star formation activity in galaxies depends on the cluster characteristics is still lacking. For example, apparently contrasting results have been found in the literature regarding the presence (Martinez et al. 2002; Biviano et al. 1997; Zabludoff & Mulchaey 1998; Margoniner et al. 2001; Goto et al. 2003) or absence (Smail et al. 1998; Andreon & Ettori 1999; Ellingson et al. 2001; Fairley et al. 2002; De Propris et al. 2004; Goto 2005; Wilman et al. 2005a) of a relation between galaxy properties and global cluster/group properties such as velocity dispersion, X-ray luminosity, and richness.

In this paper we analyze how the fraction of actively star-forming galaxies varies with environment and redshift, comparing samples of clusters and groups at $z = 0.4-0.8$ with samples in the local universe. This study is based on the ESO Distant Cluster Survey (EDisCS), a photometric and spectroscopic survey of distant clusters described in § 2. Deriving the proportion of actively star-forming galaxies as those with O II emission in EDisCS and other high-z samples (§ 3) and comparing it with low-redshift samples from the Sloan Digital Sky Survey (SDSS; § 4), we present how the fraction of star-forming galaxies evolves between $z = 0.4-0.8$ and 0 as a function of the cluster/group velocity dispersion (§ 5). In § 5.3 we discuss the incidence of O II emitters in the poorest groups and the field, and in § 5.4 we show how the distributions of the equivalent widths of O II vary with environment. Galaxy systems that strongly deviate from the trends followed by most groups/clusters are discussed in § 5.5. Star formation activity and galaxy Hubble types are compared in § 5.6. Finally, we propose a possible scenario accounting for the observed trends and discuss its major implications in § 6.

Throughout the paper, line equivalent widths and cluster velocity dispersions are given in the rest frame. We use $H_0 = 70$ km s^{-1} Mpc^{-1}, $h = H_0/100$, $\Omega_m = 0.3$, and $\Omega_\lambda = 0.7$.

2. THE EDisCS DATA SET

Our study is based on data obtained by the EDisCS, a photometric and spectroscopic survey of galaxies in 20 fields containing galaxy clusters at $z = 0.4-1$. The goal of this project is to study cluster and cluster galaxy evolution, characterizing the structure, stellar populations, internal kinematics, luminosities, and masses of galaxies in high-redshift clusters.

Candidate clusters were selected from the Las Campanas Distant Cluster Survey (LCDCS) of Gonzalez et al. (2001). Candidates were identified by the LCDCS as a surface brightness excess using a very wide filter ($\sim$4500–7500 Å). The EDisCS sample of 20 clusters was built from the 30 highest surface brightness candidates in the LCDCS, confirming the presence of an apparent cluster and of a possible red sequence with VLT 20 minute exposures in two filters (White et al. 2005).

Deep optical photometry with VLT FORS2, near-IR photometry with SOFI on the New Technology Telescope (NTT), and multislit spectroscopy with VLT FORS2 have been obtained for the 20 fields. *Hubble Space Telescope* (*HST*) Advanced Camera for Surveys (ACS) mosaic imaging of 10 of the highest redshift clusters has also been acquired (V. Desai et al. 2006, in preparation).

An overview of the goals and strategy of the survey is given in White et al. (2005), where the optical ground-based photometry is presented in detail. This consists of V, R, and I imaging for the 10 highest redshift cluster candidates, aimed to provide a sample at $z \sim 0.8$ (hereafter the high-z sample), and B, V, and I imaging for 10 intermediate-redshift candidates, aimed to provide a sample at $z \sim 0.5$ (hereafter the mid-z sample).[14] A weak-shear analysis of gravitational lensing by our clusters based on these data is presented in Clowe et al. (2006).

Typically 4 hr (high-z sample) and 2 hr exposure (mid-z sample) spectra of >100 galaxies per cluster field were obtained. Spectroscopic targets were selected from I-band catalogs. At the redshifts of our clusters this corresponds to $\sim$5000 $\pm$ 500 Å rest frame. Conservative rejection criteria based on photometric redshifts were used in the selection of spectroscopic targets to reject a significant fraction of nonmembers while retaining a spectroscopic sample of cluster galaxies equivalent to a purely I-band–selected one. A posteriori, we verified that these criteria have excluded at most 1% of the cluster galaxies (Halliday et al. 2004; B. Milvang-Jensen et al. 2006, in preparation). The spectroscopic selection, observations, and spectroscopic catalogs are presented in detail in Halliday et al. (2004) and B. Milvang-Jensen et al. (2006, in preparation).

As explained in White et al. (2005), deep spectroscopy was not obtained for two of the EDisCS fields (Cl 1122 and Cl 1238); hence, they have not been included in the present study. In the following we consider the other 18 EDisCS fields with high-quality spectroscopy. For each field, Table 1 lists the cluster name, redshift, velocity dispersion, and number of spectroscopically confirmed members of the structure that was targeted for spectroscopy and that forms the basis of our study.

3. DERIVING THE [O II] FRACTIONS IN CLUSTERS AT HIGH REDSHIFT

In this paper we wish to investigate the incidence of actively star-forming galaxies as a function of cluster velocity dispersion

[14] In practice, the redshift distributions of the high-z and the mid-z samples partly overlap, as can be seen in Table 1.

TABLE 1
EDisCS Clusters

Cluster (1)	Short Name (2)	z (3)	$\sigma \pm \delta_\sigma$ (4)	$N_{\rm mem}$ (5)	$N_{[\rm O\ II]}$ (6)	Imaging (7)	R_{200} (Mpc) (8)	$f_{[\rm O\ II]}$ (9)	$f^{\rm uncorr}_{[\rm O\ II]}$ (10)	$f^{\rm lens}_{[\rm O\ II]}$ (11)	$f^{1\ \rm Mpc}_{[\rm O\ II]}$ (12)
Cl 1232.5−1250	Cl 1232	0.5414	1080^{+119}_{-89}	54	51	*BVIJK*+	1.99	0.32 ± 0.08	0.31	0.32	0.34
Cl 1216.8−1201	Cl 1216	0.7943	1018^{+73}_{-77}	67	57	*VRIJK*+	1.61	0.53 ± 0.14	0.46	0.53	0.44
Cl 1138.2−1133.....	Cl 1138	0.4798	737^{+77}_{-56}	48	24	*VRIJK*+	1.41	0.59 ± 0.16	0.62	0.63*	0.63
Cl 1411.1−1148.....	Cl 1411	0.5201	709^{+180}_{-105}	26	18	*BVIK*	1.32	0.24 ± 0.11	0.22	0.24	0.24
Cl 1301.7−1139	Cl 1301	0.4828	681^{+86}_{-86}	37	28	*BVIK*	1.30	0.62 ± 0.15	0.61	0.61*	0.57
Cl 1354.2−1230	Cl 1354	0.7627	668^{+161}_{-80}	21	14	*VRIJK*+	1.08	0.80 ± 0.22	0.71	0.82*	0.75
Cl 1353.0−1137	Cl 1353	0.5883	663^{+179}_{-91}	22	16	*BVIK*	1.19	0.45 ± 0.17	0.44	0.34	0.34
Cl 1054.4−1146	Cl 1054−11	0.6972	589^{+78}_{-70}	49	28	*VRIJK*+	0.99	0.70 ± 0.16	0.68	0.73	0.70
Cl 1227.9−1138	Cl 1227	0.6355	572^{+96}_{-54}	22	12	*VRIJK*+	1.00	0.69 ± 0.24	0.67	0.67	0.69
Cl 1202.7−1224	Cl 1202	0.4244	540^{+139}_{-83}	21	14	*BVIK*	1.07	0.31 ± 0.14	0.29	0.31	0.31
Cl 1059.2−1253	Cl 1059	0.4561	517^{+71}_{-40}	41	28	*BVIK*	1.00	0.56 ± 0.14	0.57	0.56*	0.56
Cl 1054.7−1245	Cl 1054−12	0.7498	504^{+113}_{-65}	36	20	*VRIJK*+	0.82	0.52 ± 0.15	0.45	0.63	0.55
Cl 1018.8−1211	Cl 1018	0.4732	474^{+75}_{-57}	33	20	*BVIK*	0.91	0.56 ± 0.17	0.55	0.48*	0.46
Cl 1040.7−1155	Cl 1040	0.7043	418^{+55}_{-46}	30	13	*VRIJK*+	0.70	0.71 ± 0.23	0.69	0.71	0.71
Cl 1037.9−1243	Cl 1037	0.5789	315^{+76}_{-37}	19	8	*VRIJK*+	0.57	0.90 ± 0.33	0.88	0.92*	0.92
Cl 1103.7−1245b	Cl 1103	0.7029	242^{+126}_{-104}	11	3	*VRIJK*+	0.41	1.00 ± 0.58	1.00	...	1.00
Cl 1420.3−1236	Cl 1420	0.4959	225^{+77}_{-62}	27	9	*BVIK*	0.43	0.00 ± 0.11	0.00	0.38*	0.34
Cl 1119.3−1129.....	Cl 1119	0.5500	165^{+34}_{-19}	21	10	*BVI*	0.30	0.26 ± 0.20	0.40	0.21	0.21

Notes.—Col. (1): Cluster name. Col. (2): Short cluster name. Col. (3): Cluster redshift. Col. (4): Cluster velocity dispersion. Redshifts and velocity dispersions are taken from Halliday et al. (2004) and B. Milvang-Jensen et al. (2006, in preparation). Col. (5): Number of spectroscopically confirmed members. Col. (6): Number of members used for computing the O II fraction of col. (9). Col. (7): Available imaging. A plus sign indicates those clusters with *HST* imaging. Col. (8): R_{200} in Mpc. Col. (9): O II fraction within R_{200} corrected for completeness. Col. (10): O II fraction within R_{200} uncorrected for completeness. Col. (11): O II fraction computed within a radius R_{200} derived from the lensing estimate of σ (Clowe et al. 2006). An asterisk indicates systems with additional mass structures along the line of sight, whose lensing σ is probably overestimated. Col. (12): O II fraction computed within a radius of 1 Mpc.

and how this evolves with redshift. We do this by analyzing the proportion of galaxies with a significant O II emission line at 3727 Å, a reliable signal of ongoing star formation. Dust and metallicity variations affect significantly the *strength* of the [O II] line, and a quantitative estimate of the star formation rate from the line flux depends on slit coverage of the galaxy area and spectral extraction method. However, when the limit for line detection is sufficiently low, the simple *presence or absence* of this line in emission provides a clean estimate of the incidence of star-forming galaxies in different environments and at different redshifts.[15]

EDisCS spectra have a dispersion of 1.32 and 1.66 Å pixel^{-1} depending on the observing run, with an FWHM resolution of $\sim$6 Å, corresponding to rest frame 3.3 Å at $z = 0.8$ and 4.3 Å at $z = 0.4$. The equivalent widths of O II were measured on the spectra with a line-fitting technique that follows the one used by the MORPHS collaboration as in Dressler et al. (1999). With this method each one-dimensional spectrum is inspected interactively. Each two-dimensional spectrum was also inspected to confirm the presence of an eventual line in one dimension: this is especially useful to assess the reality of weak O II lines.

We classify as star-forming galaxies those with an equivalent width (EW) of O II less than -3 Å rest frame, adopting the convention that EWs are negative when in emission. This is a reasonable limit for galaxies with weak but still detectable current star formation activity, for example, nearby Sa galaxies. Measuring the line strength of 147 repeated spectra of galaxies (those observed more than once in different masks/runs), we find that all of them fall into either the star-forming or non–star-forming class in all repeated cases, proving that the discrimination between galaxies with EW(O II) > -3 Å and EW(O II) < -3 Å is robust from our spectra.

For each EDisCS cluster, we have computed the fraction of star-forming cluster members as the fraction of spectroscopically confirmed members[16] with a rest-frame EW([O II]) ≤ -3 Å. Error bars on the fractions have been computed using Poissonian statistics. We consider only galaxies located within the projected radius delimiting a sphere with interior mean density 200 times the critical density (R_{200}) and with an absolute V magnitude brighter than $M_{V,\rm lim}$. $M_{V,\rm lim}$ was varied with redshift between -20.5 at $z = 0.8$ and -20.1 at $z = 0.4$ to account for passive evolution. Our spectroscopy would allow an analysis for galaxies up to 0.5 mag fainter than these limits, but for this study $M_{V,\rm lim}$ was chosen to carry out a comparison with the SDSS data set (see below). Rest-frame absolute magnitudes were estimated for each EDisCS galaxy as in Rudnick et al. (2003) and are given in G. Rudnick et al. (2006, in preparation). R_{200} was computed from the cluster velocity dispersion σ as in Finn et al. (2005):

$$R_{200} = 1.73 \frac{\sigma}{1000\ \rm km\ s^{-1}} \frac{1}{\sqrt{\Omega_\Lambda + \Omega_0 (1+z)^3}}\ h^{-1}\ \rm Mpc. \quad (1)$$

The cluster center was assumed to coincide with the brightest cluster galaxy (BCG), which was identified interactively on the EDisCS VLT images. A list of the BCGs can be found in White et al. (2005). For most of the clusters, our spectroscopy samples at least out to the cluster R_{200} or beyond (Figs. 1 and 2). A few clusters have incomplete radial sampling due to their large projected radii (most notably, Cl 1232, Cl 1411, and Cl 1138),

[15] If an AGN is present, this can contribute to the emission-line flux. However, in the great majority of cases an AGN with an emission-line spectrum is associated with some level of star formation activity (e.g., Heckman et al. 1995; Cid Fernandes et al. 2004 and references therein); therefore, the contamination of the population of O II emitters from passive galaxies is bound to be negligible.

[16] After having excluded the repeated spectra of galaxies that were observed more than once.

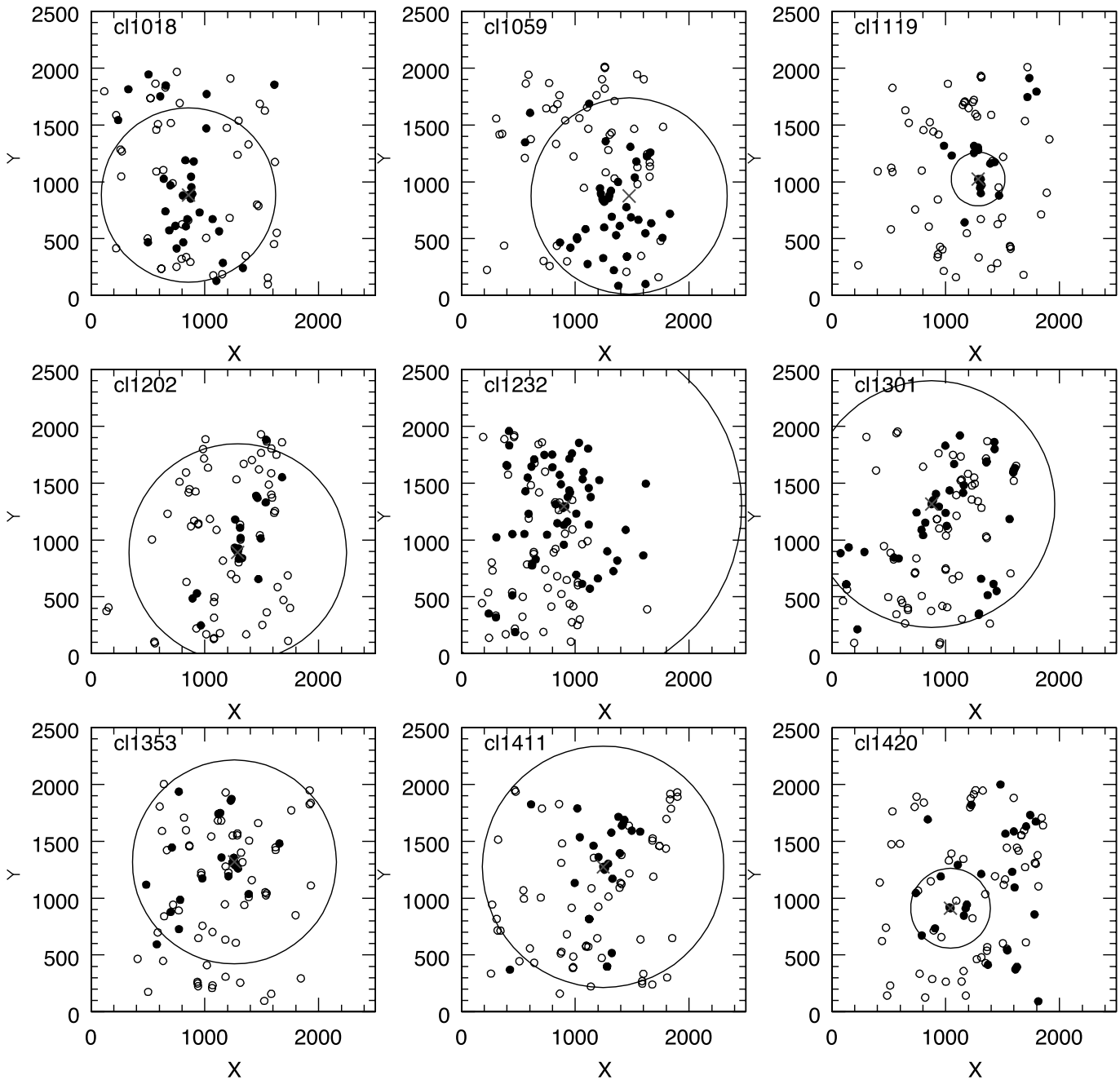

FIG. 1.—*XY* pixel positions of objects with spectra in the EDisCS mid-*z* fields. Filled circles represent spectroscopically confirmed cluster members. The circle with radius R_{200}, centered on the BCG, is shown. The axis units are pixels = 0.″2. [*See the electronic edition of the Journal for a color version of this figure.*]

or to the BCG location close to the FORS2 field edge (Cl 1227): when relevant, these cases are discussed separately.

The fractions of [O II] emitters were computed weighting each galaxy for incompleteness of the spectroscopic catalog, taking into account the completeness as a function of galaxy magnitude and position, as described in Appendix A. Ignoring these weights, however, does not affect significantly our results, as discussed in § 5. In Appendix B we show that the color distributions of the final spectroscopic sample and its parent photometric sample are indistinguishable according to a K-S test, and therefore no color bias is present in the spectroscopic sample we are using.

The exposure times of the EDisCS spectroscopy (4 and 2 hr of VLT for the high- and mid-*z* samples, respectively) were chosen to allow not only a redshift determination but also a detailed spectroscopic analysis of emission and absorption features. As a consequence, the fraction of spectroscopic targets for which no redshift could be derived is negligible: only 3% of the spectra brighter than the magnitude limit used here did not yield a redshift.[17] Hence, no correction is required to account for the success rate (percentage of spectra providing a redshift) as a function of magnitude or color.

The O II fractions derived as described above are given in column (9) of Table 1. For comparison, the table also lists the O II

[17] As discussed in Halliday et al. (2004), the spectra show that most of these are bright lower redshift galaxies (nonmembers of our clusters) observed in a red rest-frame spectral region that is featureless and thus makes it hard to derive a secure redshift.

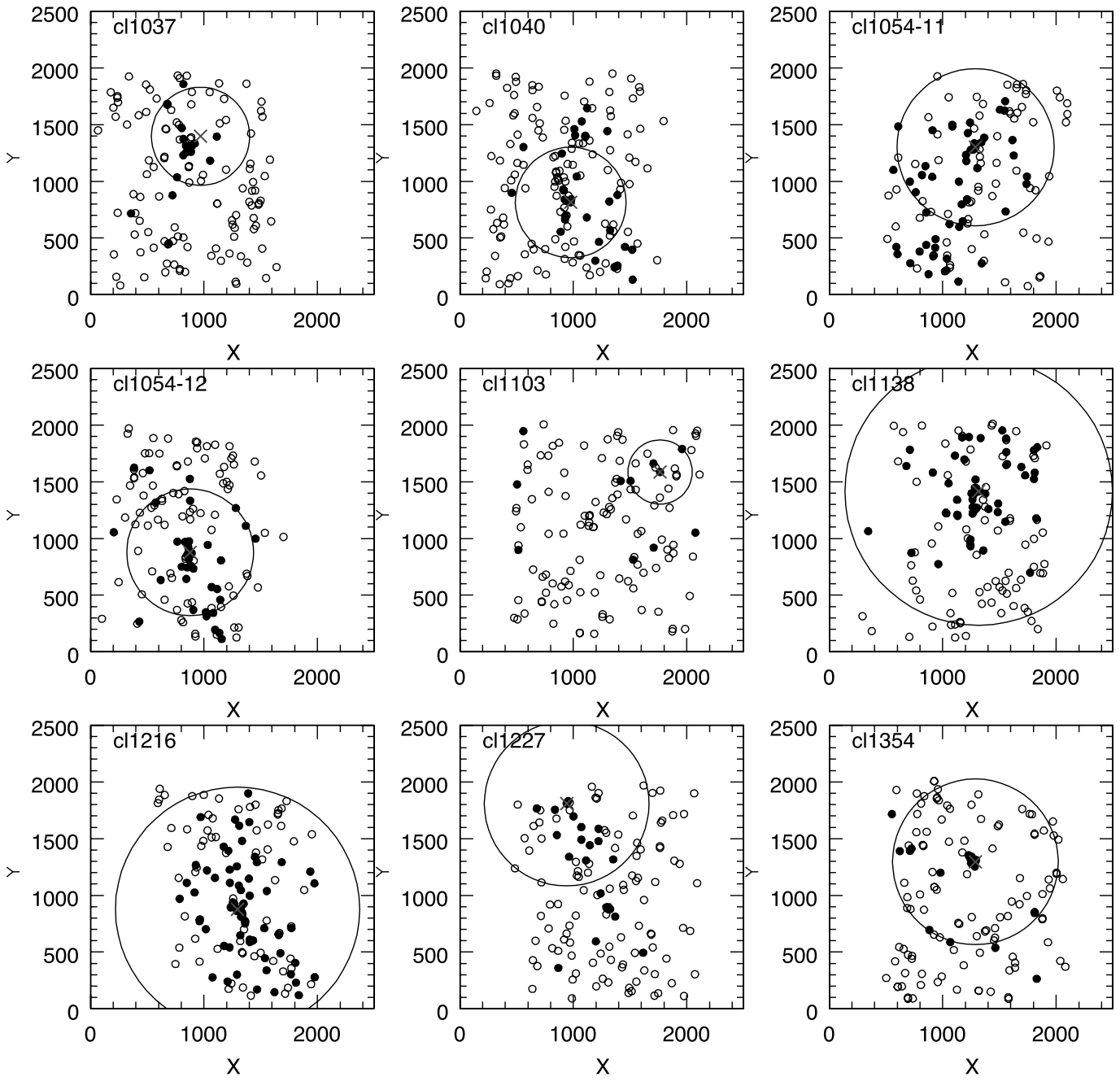

FIG. 2.—Same as Fig. 1, but for the high-z EDisCS fields. [*See the electronic edition of the Journal for a color version of this figure.*]

fractions computed without applying completeness corrections (col. [10]), or with different radial criteria: within R_{200} as derived from the σ based on the weak-lensing analysis of Clowe et al. (2006) (col. [11]) and within a fixed metric radius equal to 1 Mpc (col. [12]). For all structures except one (Cl 1420), the different estimates of the O II fraction are compatible within the errors.

3.1. *Other High-z Cluster Samples*

The EDisCS data set is homogeneous for cluster and galaxy selection and data quality; thus, an internal comparison among clusters is straightforward. A comparison with other spectroscopic surveys of distant clusters requires much more caution, as a number of conditions need to be met: such a survey should cover out to R_{200} and be representative of a magnitude-limited sample of galaxies selected in the rest frame at 4500–5500 Å. A reliable determination of the cluster velocity dispersion should be available, as well as accurate EW([O II]) measurements highly complete down to 3 Å for galaxies down to the absolute magnitude limit $M_{V,\mathrm{lim}}$. These are demanding requirements that are largely fulfilled by surveys of just a few distant clusters in the literature.

The list of additional distant clusters we include in our analysis is given in Table 2. Seven of these clusters are taken from the MORPHS survey (Dressler et al. 1999; Poggianti et al. 1999) and are at redshifts covering the low-redshift end of the EDisCS redshift range ($z = 0.38-0.55$). Two other clusters are MS 1054−03 at $z = 0.83$, taken from van Dokkum et al. (2000), and Cl 1324+3011 at $z = 0.76$, from Postman et al. (2001).

Measurements of the EW(O II) were taken from these authors, assuming that their spectroscopic catalogs are highly complete

TABLE 2
Other Distant Clusters

Cluster (1)	z (2)	$\sigma \pm \delta_\sigma$ (3)	$N_{[O\,II]}$ (4)	Imaging (5)	R_{200} (Mpc) (6)	FOV (7)	$f_{[O\,II]}$ (8)	Ref1 (9)	Ref2 (10)
Cl 1447	0.3762	838^{+163}_{-163}	21	r/i, $M_V = -19.8$	1.70	$1.2 \times 1.2\ R_{200}$	0.56±0.16	D99, P99	GM01
Cl 0024	0.3928	911^{+81}_{-107}	107	r/i, $M_V = -19.8$	1.83	$1.1 \times 1.1\ R_{200}$	0.36±0.06	D99, P99	GM01
Cl 0939	0.4060	1067^{+89}_{-96}	71	r/i, $M_V = -19.8$	2.13	$1.0 \times 1.0\ R_{200}$	0.26±0.06	D99, P99	GM01
Cl 0303	0.4184	876^{+144}_{-140}	51	r/i, $M_V = -19.8$	1.73	$1.3 \times 1.3\ R_{200}$	0.55±0.10	D99, P99	GM01
3C 295	0.4593	1642^{+224}_{-187}	25	r/i, $M_V = -19.8$	3.18	$0.7 \times 0.7\ R_{200}$	0.18±0.08	D99, P99	GM01
Cl 1601	0.5388	646^{+84}_{-87}	58	r/i, $M_V = -19.8$	1.19	$2.0 \times 2.0\ R_{200}$	0.15±0.05	D99, P99	GM01
Cl 0016	0.5459	984^{+130}_{-95}	29	r/i, $M_V = -19.8$	1.81	$1.4 \times 1.4\ R_{200}$	0.14±0.07	D99, P99	GM01
MS 1054−03	0.8315	1150^{+97}_{-97}	71	I_{814}, $M_V = -20.5$	1.78	$0.5 \times 0.8\ R_{200}$	0.31±0.06	vD00	vD00
Cl 1324+3011	0.7565	1016^{+126}_{-93}	27	R, $M_V = -20.4$	1.71	$0.3 \times 0.9\ R_{200}$	0.47±0.14	PLO01	LOP02

Notes.—Col. (1): Cluster name. Col. (2): Cluster redshift. Col. (3): Cluster velocity dispersion. Col. (4): Number of galaxy members of the cluster used for the calculation of the O II fraction. Col. (5): Photometric band used for selection of spectroscopic targets and magnitude limit we adopted to be compatible with EDisCS. Col. (6): R_{200} in Mpc. Col. (7): Field of view of the spectroscopic coverage. Col. (8): O II fraction. Cols. (9) and (10): References for the O II measurements and completeness functions and references for the cluster velocity dispersion, respectively. An additional cluster presented in Postman et al. (2001) has later been shown to be composed of four distinct clusters for which a spectroscopic catalog should become available in the future (Gal & Lubin 2004). A cluster from Postman et al. (1998) was not included because its completeness function was not available. The cluster and the group at $z = 0.59$ in the MS 2053 field of Tran et al. (2005) have $\sigma = 865$, $f_{[O\,II]} = 0.34$ and $\sigma = 282$, $f_{[O\,II]} = 0.67$, respectively, where $f_{[O\,II]}$ is given by the authors for galaxies with EW(O II) < -5 Å, down to approximately the same galaxy magnitude limit and radius adopted here. Since their EW limit is higher than the 3 Å limit we have used, we decided not to include these structures in Fig. 4, but we note that these points would roughly follow the trend of the other distant clusters in the plot. Any other cluster from the literature at $z \geq 0.4$ could not be included because it was missing one or more necessary pieces of information (O II catalogs, completeness information, etc.).

References.—(D99) Dressler et al. 1999; (P99) Poggianti et al. 1999; (vD00) van Dokkum et al. 2000; (PLO01) Postman et al. 2001; (GM01) Girardi & Mezzetti 2001; (LOP02) Lubin et al. 2002.

for EW(O II) < -3 Å. This is the case for the MORPHS sample, as discussed in Dressler et al. (1999), and appears to be a reasonable assumption also for van Dokkum et al. (2000) and Postman et al. (2001), given the EW distributions and error bars in their catalogs. These samples were weighted for incompleteness using the completeness functions provided by the authors (Table 2). Galaxies were included in the O II computation if brighter than the closest available apparent magnitude limits corresponding to the absolute magnitude limits adopted for EDisCS, as a function of redshift. The radial coverage for these clusters in units of R_{200} is shown in Table 2. We note that the spectroscopic sample of the Postman et al. (2001) cluster was selected in rest-frame U band, while the EDisCS and all other clusters used in this analysis were selected at $\sim$5000 ± 500 Å rest frame. Although the estimate of the O II fraction in clusters in these external samples cannot be carried out in a way that is fully homogeneous with the analysis performed on the EDisCS data, due to the slight differences in radial coverage, magnitude limit, and so on, such differences are sufficiently small to allow an interesting comparison with the EDisCS data: this is presented in § 5.

4. THE [O II] FRACTIONS AT LOW REDSHIFT: SDSS

In order to compare with clusters at low redshift, we constructed a local comparison sample from the spectroscopic SDSS. Rather than trying to obtain a sample with the largest possible number of clusters, we aimed to build a sample with selection criteria similar to EDisCS. For simplicity, we used the Abell cluster catalog. Its selection is based on (projected) overdensities of galaxies, which can be regarded as being similar to the selection of EDisCS clusters, that were chosen by their light excess over the background.

Our Abell sample was built according to the following steps:

1. At the time of sample selection, the most comprehensive compilation of properties of Abell clusters was by Struble & Rood (1991). From this, we selected clusters with a redshift estimate based on at least two galaxies. This yields 774 clusters.

2. Only clusters with $0.04 < z < 0.085$ were selected. This reduces the sample to 227 clusters. The lower limit in redshift is chosen to reduce fiber aperture effects. At $z > 0.04$, the SDSS fibers sample a significant fraction of the galaxy light, and the spectral classification into star-forming and non–star-forming galaxies should not differ significantly from the integrated spectral class (Kewley et al. 2005). The upper redshift limit is imposed by the need to have spectra for galaxies down to a sufficiently deep absolute magnitude, for comparison with EDisCS. Above $z = 0.085$, the SDSS spectroscopy samples only the bright end of the galaxy luminosity function, galaxy numbers per cluster become too small, and errors on the O II fraction are too high to reach solid conclusions.

3. For each cluster, we identify galaxies from the spectroscopic SDSS DR2 catalog that lie within one Abell radius ($R_A = 1.'7/z$) from the cluster center quoted by Struble & Rood (1991). Only clusters with at least 20 matched galaxies are retained (32 clusters).

4. At this stage, the image of each cluster was inspected interactively. We restricted the sample to clusters that are well separated from the survey boundaries, and we identified a BCG from the SDSS imaging data. Redshift histograms were also inspected to verify the presence of a concentration of galaxies at the redshift given by Struble & Rood (1991). These constraints yield a sample of 24 clusters, to which we add two clusters with redshifts slightly lower than 0.04 and two with redshifts slightly higher than 0.085. The final list of 28 clusters is presented in Table 3.

5. As for the EDisCS sample, we rely on the biweight estimator of Beers et al. (1990) for determining the cluster redshift and velocity dispersion, as described in Appendix C.

Once our low-redshift comparison sample was selected, a number of steps were taken to ensure a meaningful comparison with our high-z sample:

1. The SDSS spectroscopic target selection was performed in the r band ($r < 17.7$). In order to more closely approximate the

TABLE 3
SDSS Clusters

Cluster (1)	z (2)	$\sigma \pm \delta_\sigma$ (3)	$N_{[O\,II]}$ (4)	R_{200} (5)	$f_{[O\,II]}$ (6)	$f^{uncorr}_{[O\,II]}$ (7)
A2255.....	0.0801	1151±64	106	2.74	0.22±0.05	0.24
A1767.....	0.0707	908±54	48	2.17	0.19±0.06	0.19
A85.....	0.0555	861±48	46	2.07	0.16±0.06	0.17
A160.....	0.0425	842±64	25	2.04	0.29±0.11	0.28
A1066.....	0.0691	833±62	39	1.99	0.31±0.09	0.31
A2670.....	0.0761	804±48	53	1.92	0.28±0.08	0.30
A1650.....	0.0837	770±72	32	1.83	0.17±0.08	0.22
A1809.....	0.0794	730±55	37	1.74	0.16±0.07	0.16
A628.....	0.0838	667±67	24	1.58	0.54±0.14	0.50
A1424.....	0.0755	664±53	33	1.58	0.21±0.08	0.21
A2593.....	0.0417	659±52	13	1.60	0.07±0.08	0.08
A1564.....	0.0792	600±63	19	1.43	0.17±0.11	0.21
A2197.....	0.0303	586±27	31	1.43	0.25±0.09	0.26
A117.....	0.0551	570±46	17	1.37	0.30±0.13	0.29
A1559.....	0.1056	541±86	8	1.27	0.31±0.18	0.25
A933.....	0.0969	515±55	15	1.22	0.26±0.13	0.27
A1780.....	0.0776	500±63	18	1.19	0.25±0.12	0.28
A1452.....	0.0616	485±105	7	1.16	0.42±0.25	0.43
A116.....	0.0667	471±71	4	1.13	0.47±0.35	0.50
A2448.....	0.0820	466±81	11	1.11	0.28±0.16	0.27
A1468.....	0.0850	464±105	16	1.10	0.38±0.15	0.38
A1139.....	0.0393	436±46	10	1.06	0.38±0.20	0.40
A1507.....	0.0599	419±47	11	1.01	0.54±0.22	0.55
A2630.....	0.0669	402±69	9	0.96	0.32±0.19	0.30
A1218.....	0.0801	365±77	7	0.87	0.55±0.29	0.57
A1171.....	0.0748	352±51	5	0.84	0.67±0.35	0.60
A1534.....	0.0699	333±39	11	0.80	0.18±0.13	0.18
A1279.....	0.0544	192±37	3	0.46	1.00±0.58	1.00

Notes.—Col. (1): Cluster name. Col. (2): Cluster redshift. Col. (3): Cluster velocity dispersion. Col. (4): Number of members used for computing the O II fraction. Col. (5): R_{200} in Mpc. Col. (6): O II fraction corrected for completeness. Col. (7): O II fraction uncorrected for completeness.

rest-frame EDisCS selection wavelength, we extracted a g-selected sample from the SDSS spectroscopic catalogs. This corresponds to the subset of galaxies with $g \leq 18$: brighter than this limit, 99% of the galaxies have $r < 17.7$ and their g magnitude distribution follows closely the distribution in the whole g-band photometric sample. Galaxies brighter than $g = 12$ and $r = 12$ were excluded, being brighter than any cluster member of the clusters considered. Therefore, the SDSS spectroscopic sample we used is the subset of the SDSS catalogs with $12 < r < 17.7$ and $12 < g < 18.0$.

2. Each galaxy in the spectroscopic catalog was assigned completeness weights as a function of magnitude and position comparing, cluster by cluster, the number of galaxies in the SDSS spectroscopic and photometric (g band) catalogs, as done for EDisCS (see Appendix A). As in EDisCS, essentially all targeted galaxies (99.9%) yield a reliable redshift (Strauss et al. 2002); thus, no correction is required to account for the spectroscopic success rate.

3. The analysis of the fraction of [O II] emitters was carried out on the SDSS data as for EDisCS. The center of each cluster was assumed to coincide with the BCG. Only galaxies within R_{200} were considered, down to an absolute V magnitude limit of -19.8, corresponding to the limit at which spectroscopic incompleteness sets in at these redshifts in the SDSS sample. This limit was used to determine the absolute magnitude limit in the distant clusters, once passive evolution was taken into account. Galaxy absolute V magnitudes were obtained from the absolute Petrosian magnitudes in the SDSS system using the transformation of Blanton.[18]

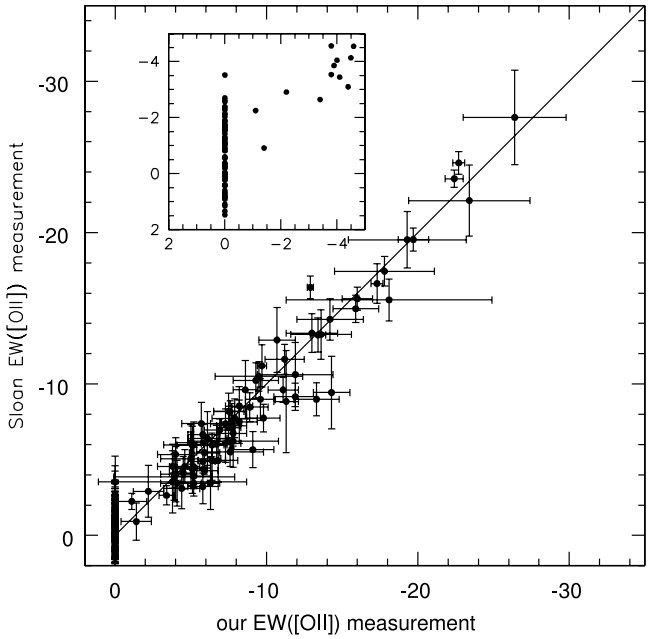

Fig. 3.—EW(O II) values of SDSS spectra in plate 973. The measurement obtained with the EDisCS method is compared with the EW listed by SDSS. The inset is a blowup of the lower left corner of the plot, in which error bars are omitted for clarity. In this plot, EDisCS EWs equal to 0 correspond to those spectra in which the line is not detected and the spectral fluctuations in that region are considered noise. Since the SDSS measurements are fully automatic, these cases can yield a nonnull negative or positive EW value, which is, however, consistent with zero within the error bar in most cases.

4. The star-forming fraction was computed as the fraction of galaxies with EW(O II) < -3 Å rest frame. The O II EWs of the SDSS spectra were taken from Brinchmann et al. (2004a, 2004b). Since these were measured with a different routine than the one we used for EDisCS, we first tested the consistency between the SDSS and our EW measurements on all of the 162 spectra of a random SDSS plate (plate 973). The comparison is shown in Figure 3, where a good agreement is visible. Since our purpose is to obtain a meaningful comparison of the fraction of galaxies with EW(O II) < -3 Å, we are mainly interested in those eventual cases of discrepancy between our and the SDSS measurement that could cause a different classification (star-forming vs. non–star-forming). We find that in 99% of the cases our EW measurements agree with the SDSS EWs for the purpose of dividing galaxies into greater than and less than -3 Å.[19] We conclude that using the EWs by Brinchmann et al. (2004a) does not introduce any systematics in the comparison with the high-redshift clusters, and we use their EW measurements to compute the O II fraction in low-z clusters. O II fractions computed with and without completeness corrections, together with redshifts, velocity dispersions, R_{200}, and number of spectroscopically confirmed cluster members used to compute the O II fractions, are listed for our Abell-SDSS clusters in Table 3.

To test our results on a larger control sample that, however, resembles less closely the EDisCS sample for selection and

[18] See http://astro.physics.nyu.edu/~mb144/kcorrect/linear.ps.

[19] As visible in the inset of Fig. 3, only two cases of small discrepancy are found among the 162 galaxies: galaxy 506 with EW(SDSS) $= -2.6 \pm 0.6$ Å and EW(EDisCS) $= -3.4 \pm 0.5$ Å, and galaxy 369 with EW(SDSS) $= -3.5 \pm 1.1$ Å and EW(EDisCS) $= 0$ Å, because no line appears to be present from a visual inspection of the spectrum.

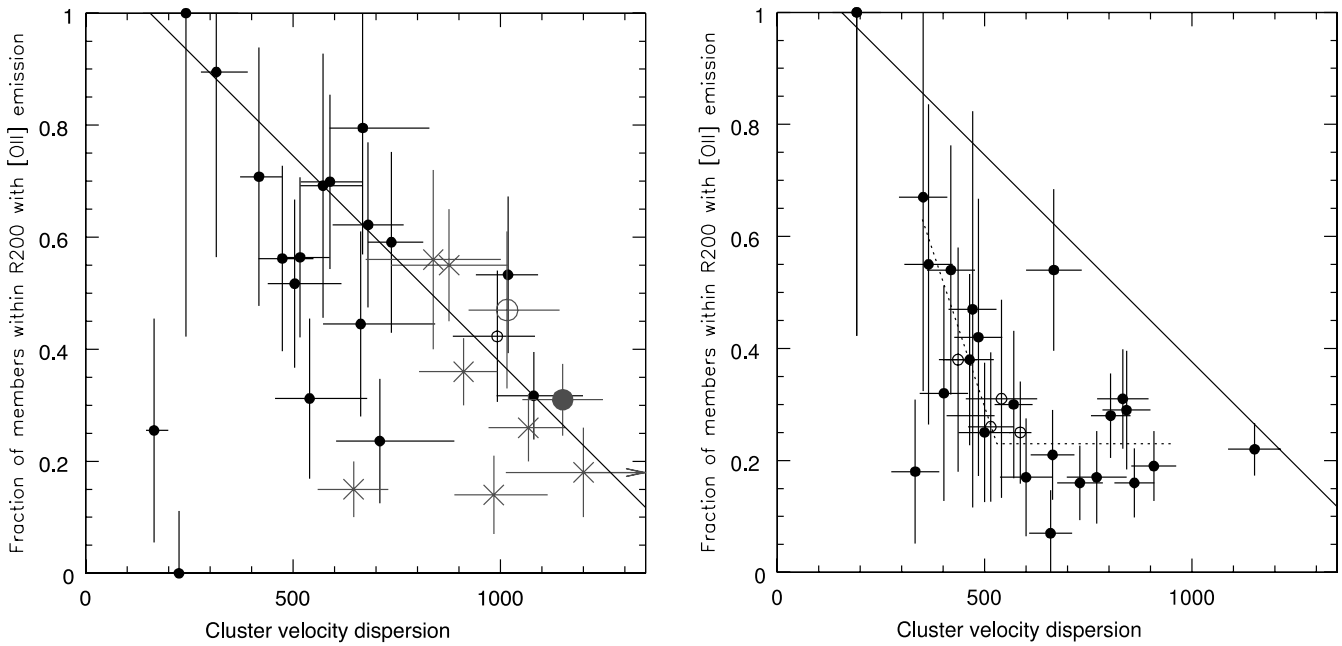

FIG. 4.—*Left*: O II–σ relation in clusters at $0.4 \leq z \leq 0.8$. The fraction of cluster members within R_{200} with O II emission is plotted vs. the cluster velocity dispersion. Filled circles represent EDisCS data points in each one of the 18 fields, as in Table 1. The crosses are for MORPHS clusters; the large filled circle is the cluster MS 1054−03 from van Dokkum et al. (2000), and the large open circle is Cl 1324+3011 from Postman et al. (2001). Error bars on the fractions are Poissonian. The solid line across the plot is taken as a description of the upper envelope of the high-z points (see text). The same line is repeated in the right panel, to illustrate the differences. At high z, the majority of systems group around this line, while at low z (*right panel*) the great majority fall well below the line. *Right*: O II–σ relation in low-redshift clusters from SDSS described in § 4. Open circles indicate those SDSS clusters slightly outside of the preferred redshift range. The two dashed lines represent the eye-fitted most heavily populated region in the plot. [*See the electronic edition of the Journal for a color version of the left panel of this figure.*]

characteristics, we also chose a second cluster sample in the SDSS from the C4 catalog of Miller et al. (2005) at redshift $0.04 \leq z \leq 0.08$. The purity of the C4 sample is discussed in Miller et al. (2005). Such a sample is more prone to be contaminated by filaments, sheets, and multiple structures yielding an overestimated σ. To minimize the contamination of structures with severely overestimated velocity dispersion, we retained only clusters with $\sigma \leq 1500$ km s^{-1}, $\sigma \leq \sigma_{C4} + 200$ km s^{-1}, and a number of galaxies within 3 σ from the cluster redshift and within R_{200} equal to or greater than 7, where σ was measured from the SDSS spectroscopic tables as described in Appendix C and σ_{C4} is the velocity dispersion given by Miller et al. (2005). Clusters with clear multiple peaks in the redshift histograms indicating that the σ is unreliable were excluded.

Since all but one of the EDisCS structures have at least eight members within these magnitude and radial limits ($N_{[O\,II]}$ in Table 1), we included only C4 clusters with at least eight members usable to compute the O II fraction. Our final C4-based sample consists of 88 clusters, whose centers were taken to coincide with the BCG listed by Miller et al. (2005).[20] The O II fraction of these clusters was computed from a g-selected sample of galaxies within R_{200} and with $M_V < -19.8$, as it was done for the Abell sample. For the C4-based sample we did not apply completeness weights, given that these corrections did not affect significantly the O II fractions of the Abell clusters (see Table 3).

5. RESULTS

5.1. *Star Formation Activity at High Redshifts as a Function of the Cluster Mass*

Our main result is shown in Figure 4. The left panel presents the fraction of O II emitters as a function of cluster velocity dispersion for EDisCS clusters (*filled small circles*) and for the other clusters at $z = 0.4-0.8$ whose data were taken from the literature as described in § 3.1.

Most data points occupy a stripe in this diagram, indicating that most clusters follow a broad anticorrelation between the fraction of star-forming galaxies and the cluster velocity dispersion: generally, more massive clusters have a lower fraction of star-forming galaxies. When including all clusters, a Kendall test shows that an anticorrelation between cluster velocity dispersion and star-forming fraction is present with a 97.1% probability. There are evident outliers that do not follow the [O II]–σ trend defined by the majority of clusters. The most evident outliers are Cl 1119 and Cl 1420, two groups with $\sigma < 400$ km s^{-1} that are discussed further in § 5.5. The Kendall probability becomes 99.9% when excluding these two outliers. The probabilities excluding non-EDisCS data points become 48.0% and 96.2% when the two outliers are included and excluded, respectively.

Assuming that the cluster velocity dispersion is related to the mass of the system,[21] the [O II]–σ relation shown in the left panel of Figure 4 suggests that it is the mass of the system, although

[20] The BCG was chosen by Miller et al. (2005) to be the brightest entry in the SDSS catalog within 500 h^{-1} kpc from the peak of the C4 density field, with EW(Hα) > -4 Å and within 4 σ from the cluster redshift, or with no spectroscopy but brighter than $m_r = 19.6$ and $M_r = -19.8$ with colors lying within the cluster color-magnitude sequence and no more than 2 mag dimmer than the BCG identified based on the 4 σ criterion.

[21] We note that two EDisCS clusters, Cl 1216 and Cl 1232, show evidence for substructure and therefore in principle their velocity dispersions may be a poor indicator of their masses (Halliday et al. 2004). However, a subsequent weak-lensing analysis of EDisCS clusters has shown that substructure does not strongly affect the spectroscopic measurement of their velocity dispersion, confirming within the errors the spectroscopic estimate of σ ($\sigma = 1152^{+70}_{-78}$ for Cl 1216, and $\sigma = 948^{+50}_{-55}$ for Cl 1232; Clowe et al. 2006).

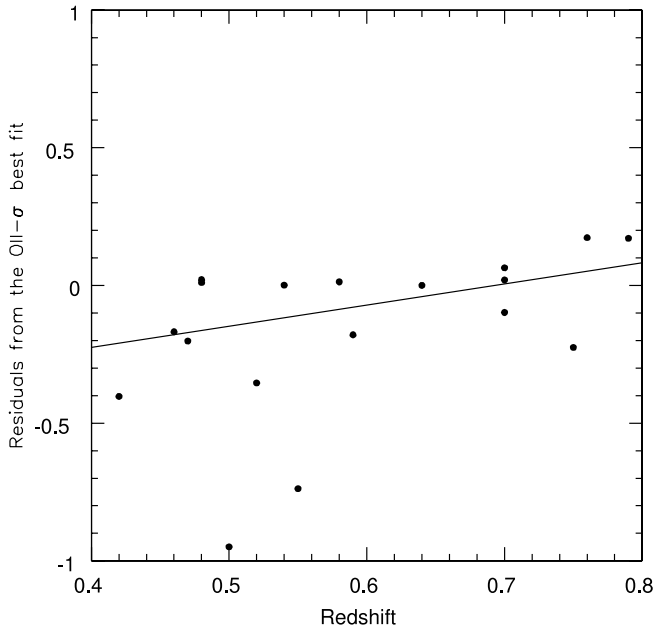

FIG. 5.—Residuals of the O II fraction of EDisCS clusters with respect to the line drawn in the O II–σ relation at high z shown in Fig. 4, plotted vs. cluster redshift. The solid line is the least-squares fit having excluded the two outliers (Cl 1119 and Cl 1420), which are the two points with residuals less than −0.5.

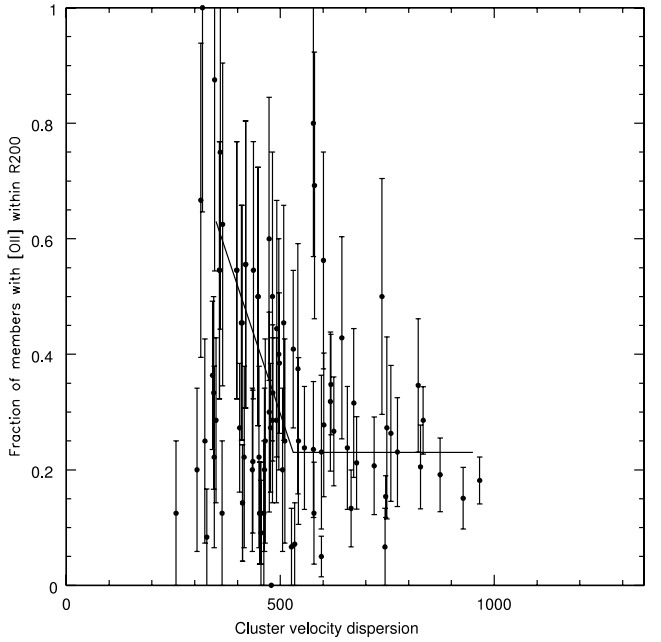

FIG. 6.—O II–σ relation in SDSS clusters at $0.04 < z < 0.08$ taken from the C4 catalog (Miller et al. 2005). Error bars on the σ have been omitted for clarity. The two lines indicate the trend followed by the Abell sample, as the dashed lines in the right panel of Fig. 4.

with a significant scatter, that largely determines what proportion of its member galaxies are forming stars at $z \sim 0.6$. Given the scatter and the outliers in this plot, however, it is uncertain whether this is better described as a broad relation between the O II fraction and σ or as an upper envelope. In fact, the most notable feature of this diagram is the absence of data points in the upper right corner, above the most populated stripe. This envelope in the O II fraction versus σ plane seems to imply that at $z = 0.4-0.8$ a system of a given mass can have *at most* a certain fraction of star-forming galaxies or, equivalently, must have *at least* a given fraction of galaxies that are already passive at this epoch. More massive systems have a lower maximum-allowed fraction of star-forming galaxies or, equivalently, a higher minimum-allowed fraction of passive galaxies.

The solid line in Figure 4 is a "hand-drawn" description of this upper envelope:[22]

$$f_{[\mathrm{O\,II}]} = -0.74\left(\frac{\sigma}{1000\ \mathrm{km\ s^{-1}}}\right) + 1.115. \quad (2)$$

When plotting the residuals from this relation for EDisCS clusters as a function of cluster redshift (Fig. 5), there is a trend of increasing O II fraction toward higher redshifts in the interval $z = 0.4-0.8$. Since within our sample there is no correlation between cluster redshift and velocity dispersion (see Table 1), Figures 4 and 5 indicate that both a trend of the O II fraction with σ and one with redshift are present. In the next subsection we investigate the evolution with redshift in more detail, comparing these results with our SDSS cluster sample.

5.2. *Evolution of the* O II–σ *Relation in Clusters*

The [O II]–σ trend observed in distant clusters can be compared with nearby clusters to quantify the evolution with redshift of the star-forming fraction in clusters as a function of the system velocity dispersion. The right panel of Figure 4 shows that SDSS Abell clusters at $z \sim 0.04-0.08$ have significantly lower fractions of star-forming galaxies than clusters at $z \sim 0.4-0.8$. The solid line in this diagram is the same as the solid line in the left panel and corresponds to the line following the high-z data points. While at high z most clusters fall around this line (*left panel*), at low z the great majority of clusters fall well below this line (*right panel*).

At low z, an approximate description of the data points in the O II–σ diagram is given by the two dashed lines in Figure 4 (*right panel*), as follows:

$$f_{[\mathrm{O\,II}]} = \begin{cases} -0.0022\sigma + 1.408, & \sigma < 530, \\ 0.23, & \sigma > 530. \end{cases} \quad (3)$$

In fact, the average O II–σ relation is flat for $\sigma > 550$ km s^{-1}; no clear trend seems to be present above this velocity dispersion. In contrast, a trend is visible at $\sigma < 500$ km s^{-1}, with the O II fraction rising for most systems toward lower velocity dispersions. The average $f_{[\mathrm{O\,II}]}$ in 3 bins of velocity dispersion for $\sigma < 550$ km s^{-1} increases from 0.31, to 0.41, to 0.54 going to lower σ. A Kendall test shows the trend below 600 km s^{-1} to be significant at the 98.5% level.

The rather small low-z sample we use here, being quality controlled and comparable to EDisCS, shows significant differences with respect to the high-z clusters. It is interesting to compare the results obtained for this sample with those obtained for the C4 control sample. The results for C4 clusters are shown in Figure 6. These clusters confirm the main trends observed in the Abell sample: for $\sigma > 550$ km s^{-1}, the O II fraction does not seem to depend on σ and is smaller than 0.3 for the great majority of clusters. At $\sigma \leq 500$ km s^{-1}, many systems have an $f_{[\mathrm{O\,II}]}$ higher than 0.3, although there are also systems with low σ and low $f_{[\mathrm{O\,II}]}$. While from the Abell sample there appears to be a trend of increasing average O II fraction toward lower velocity dispersions,

[22] This line is taken to be equal to a fit to the EDisCS points, after excluding the two group outliers, using an M estimate that minimizes absolute deviations (Press et al. 1986).

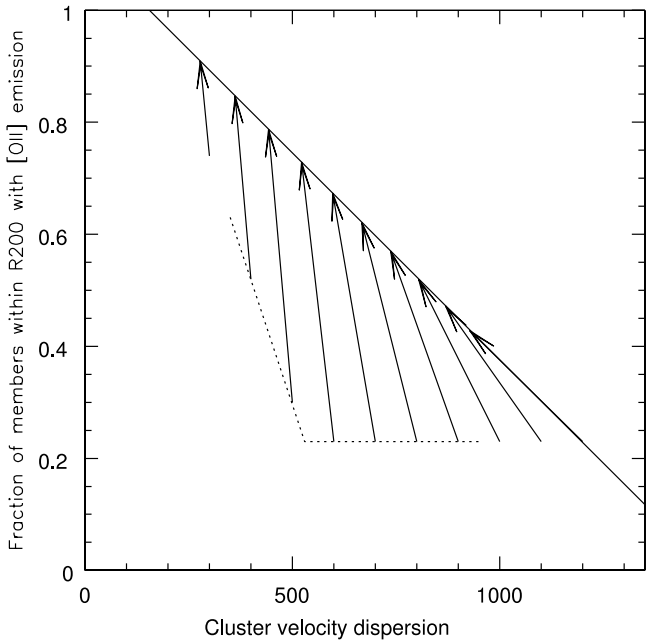

FIG. 7.—Evolution of the O II–σ relation inferred from observations at different redshifts. The solid line and the two dashed lines represent the observed relations followed by the majority of clusters at high and low z, respectively. These are the same lines shown in the left and right panels of Fig. 4. The arrows identify the average progenitors at $z = 0.6$ of clusters of different mass at $z = 0$ as expected from simulations, considering the fact that the cluster mass and hence its velocity dispersion evolve too (see text for details). If σ did not evolve with time, the arrows would be vertical in this plot.

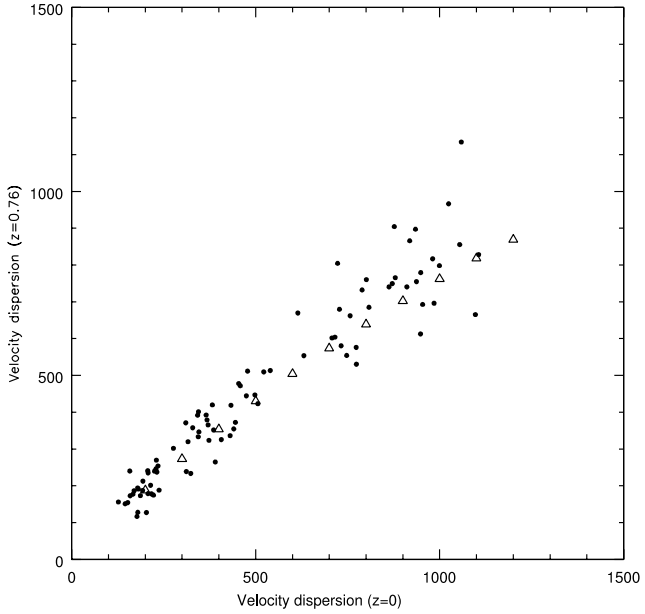

FIG. 8.—Relation between the velocity dispersion of systems at $z = 0$ and at $z = 0.76$. Open triangles are average values derived analytically from Wechsler et al. (2002) and eq. (4), as described in § 5.2. Filled circles are results for 90 halos from the MS (Springel et al. 2005), as described in § 5.2.

for the C4 clusters it is unclear whether there is a trend at $\sigma < 500$ km s^{-1} or simply a large scatter in the O II fraction at low σ. We note that the trend of rising average $f_{[\mathrm{O\,II}]}$ observed in the Abell sample is in excellent agreement with the results of Martinez et al. (2002), who found the average fraction of emission-line galaxies to decrease monotonically with virial mass for groups (10^{12}–2×10^{14} $M_\odot$) from the Two Degree Field Galaxy Redshift Survey (2dFGRS). The result from Martinez et al. (2002) parallels the trend of increasing early-type fractions toward higher velocity dispersion in the poor groups studied by Zabludoff & Mulchaey (1998), who noted that the early-type fractions in the most massive groups of their sample were comparable to those found in rich clusters. A rising fraction of "late-type galaxies" (defined on the basis of their color and star formation from emission lines) toward lower velocity dispersions is also found below 500 km s^{-1} in SDSS groups by Weinmann et al. (2006). Our low-z trends also agree with the fraction of passive galaxies in 2dF groups from Wilman et al. (2005b, see their Fig. 7).[23] Keeping in mind the caveat of a larger scatter in the C4 sample at low σ, in the following we adopt as reference the rising trend observed in the Abell sample. As seen below, this does not influence our main conclusions.

In fact, the most relevant and striking aspect of the Abell and C4 comparison is that both samples show a break in the behavior of the O II fraction with σ at the same velocity dispersion ($\sim$500 km s^{-1}) and that most clusters above this σ have a fraction of star-forming galaxies around 20%. As discussed below, this critical threshold in σ is an important observational landmark for inferring the effects of the environment on galaxy star formation histories.[24]

A schematic view of the evolution in the O II–σ diagram is presented in Figure 7. The solid line and the two dashed lines illustrate the position of the most densely populated regions at high and low redshift, respectively, reproducing the average observed trends followed by most clusters in the two panels of Figure 4.

The arrows in Figure 7 indicate the average velocity dispersion of $z = 0.6$ progenitors of systems of different masses at $z = 0$. This was computed from the assembly history given by high-resolution N-body simulations by Wechsler et al. (2002), adopting concentration parameters as in Bullock et al. (2001) and computing the relation between mass of the system and σ as in Finn et al. (2005):

$$M^{\mathrm{sys}} = 1.2 \times 10^{15} \left(\frac{\sigma}{1000 \text{ km s}^{-1}} \right)^3 \times \frac{1}{\sqrt{\Omega_\Lambda + \Omega_0 (1+z)^3}} \; h^{-1} \; M_\odot. \quad (4)$$

In Figure 8, the mean change of σ between $z = 0$ and 0.76 derived in this way (*open symbols*) is compared with the evolution obtained from the Millennium Simulation (MS; Springel et al. 2005). Filled symbols represent results for 90 halos at $z = 0$ extracted from the MS and followed back in time by tracking at each previous redshift their most massive progenitor. The MS follows $N = 2160^3$ particles of mass 8.6×10^8 h^{-1} $M_\odot$ within a comoving box of size 500 h^{-1} Mpc on a side and with a spatial resolution of 5 h^{-1} kpc. We extracted 90 halos within the simulation box, uniformly distributed in log (mass) between

[23] For clusters, Biviano et al. (1997) also found a trend with σ in the fraction of emission-line galaxies in the ESO Nearby Abell Cluster Survey between 400 and 1100 km s^{-1}. A direct comparison with our results cannot be carried out, due to the very different threshold of line strength adopted for identifying emission-line galaxies, but they found that on average the mean emission-line fraction in three bins of σ decreased toward higher σ. If we analyzed the O II fraction for our SDSS clusters in three similarly wide bins of σ, instead of presenting the results cluster by cluster, we would obtain a similar trend.

[24] We note that our low-z samples are composed for the great majority of structures with σ between 350 and 900 km s^{-1}; therefore, they do not allow an exploration of the properties of the most massive and the least massive systems.

TABLE 4

MEAN EVOLUTION BETWEEN $z = 0$ AND 0.6 OF THE VELOCITY DISPERSION σ, THE MASS OF THE SYSTEM M^{sys}, AND THE O II FRACTION

$\sigma_{z=0}$ (km s^{-1}) (1)	$M^{sys}_{z=0}$ ($h^{-1}\,M_\odot$) (2)	$f_{[O\,II]_{z=0}}$ (3)	$\sigma_{z=0.6}$ (km s^{-1}) (4)	$M^{sys}_{z=0.6}$ ($h^{-1}\,M_\odot$) (5)	$f_{[O\,II]_{z=0.6}}$ (6)	Δf (7)
1200.....	2.1×10^{15}	0.23	928	6.9×10^{14}	0.45	0.22
1100.....	1.6×10^{15}	0.23	869	5.7×10^{14}	0.49	0.26
1000.....	1.2×10^{15}	0.23	805	4.5×10^{14}	0.54	0.31
900.....	8.8×10^{14}	0.23	737	3.5×10^{14}	0.58	0.35
800.....	6.1×10^{14}	0.23	668	2.6×10^{14}	0.63	0.40
700.....	4.1×10^{14}	0.23	597	1.8×10^{14}	0.68	0.45
600.....	2.6×10^{14}	0.23	522	1.2×10^{14}	0.73	0.50
500.....	1.5×10^{14}	0.30	443	7.5×10^{13}	0.79	0.49
400.....	7.7×10^{13}	0.52	362	4.1×10^{13}	0.85	0.33
300.....	3.2×10^{13}	0.74	278	1.9×10^{13}	0.91	0.17
200.....	9.6×10^{12}	0.96	190	5.9×10^{12}	0.97	0.01
100.....	1.2×10^{12}	1.00	98	0.8×10^{12}	1.00	0.00

NOTES.—Col. (1): Velocity dispersion of a system at $z = 0$. Col. (2): Corresponding mass of the system at $z = 0$ in units of $h^{-1}\,M_\odot$. The relation between $\sigma_{z=0}$ and the mass is computed according to eq. (4). Col. (3): Average O II fraction at $z = 0$ for a system of $\sigma_{z=0}$, derived from eq. (3). Col. (4): Mean velocity dispersion at $z = 0.6$ of a system with $\sigma_{z=0}$ as in col. (1). Here $\sigma_{z=0.6}$ is computed from col. (5) according to eq. (4). Col. (5): Mean mass at $z = 0.6$ of a system with $M_{z=0}$ as in col. (2). The relation between mean mass at $z = 0$ and mean mass at $z = 0.6$ is computed according to Wechsler et al. (2002) (see § 5.2). Col. (6): Average O II fraction at $z = 0.6$ for a system of $\sigma_{z=0.6}$ as in col. (4), derived from eq. (2). Col. (7): Difference between the O II fractions at $z = 0.6$ and $z = 0$ (col. [6] minus col. [3]).

5×10^{12} and $5 \times 10^{15}\,M_\odot$. Dark matter halos were populated using the semianalytic model presented in De Lucia et al. (2006; see also Croton et al. 2006). For each halo, we considered all galaxies within $2R_{200}$ from the central galaxy to compute the projected velocity dispersion along the *x*-, *y*-, and z-axes. In Figure 8 we have plotted the mean of these projected velocity dispersions.

Figure 8 shows a very good agreement between the evolution of the velocity dispersions estimated from the two independent simulations. In the following, we use the average evolution of σ derived from Wechsler et al. (2002) and equation (4) to establish the evolutionary link between low- and high-z structures.[25] In Table 4 we list the average $f_{[O\,II]}$ fractions observed at high and low redshift as a function of the cluster velocity dispersion and mass at $z = 0$, the corresponding average σ and mass of that structure at $z = 0.6$, and the difference Δf in $f_{[O\,II]}$ between the two redshifts.[26]

Figure 7 and Table 4 show that the strongest evolution in mass and in velocity dispersion is expected for the most massive structures. The same figure and table also illustrate that the observed change in star-forming fraction between $z = 0.6$ and 0 is maximum instead for intermediate-mass structures, those with $\sigma \sim 5-600$ km s^{-1} at $z = 0$ and $\sim$450–500 km s^{-1} at $z = 0.6$. The evolution is smaller at both higher and lower masses but is still significant even for the most massive systems in the SDSS sample.[27] In the mass range we observe, the change in the average star-forming fraction Δf ranges between 20%–30% and 50%.

It is essential to keep in mind that the trends in Figure 7 and Table 4 depict an average evolution apparently followed by the majority of systems, but a large scatter is present in the observed O II–σ relation at all redshifts, and the evolution of the cluster masses is expected to proceed with a significant scatter too, as shown in Figure 8.

In this section we have shown that the fraction of star-forming (and, conversely, passive) galaxies in clusters has evolved significantly between $z \sim 0.6$ and 0. For the first time, we can quantify how the average evolution varies with the mass of the system. Why the proportion of passive/star-forming galaxies broadly correlates/anticorrelates with the velocity dispersion of the system for most clusters at high z, why this proportion evolves with redshift, why the evolution is maximum for intermediate-mass systems, and why there is no clear trend with σ at $z = 0$ for systems more massive than $\sim$550 km s^{-1} are questions that are addressed in § 6.

TABLE 5

OTHER EDISCS STRUCTURES

Cluster (1)	z (2)	$\sigma \pm \delta_\sigma$ (3)	N_{mem} (4)	$N_{[O\,II]}$ (5)	$f_{[O\,II]}$ (6)	Distance/σ (7)
C2_1138.....	0.4549	529^{+109}_{-54}	11	8	0.38±0.22	7
C2_1227.....	0.5822	432^{+225}_{-81}	11	8	0.88±0.33	17
G1_1301.....	0.3971	393^{+84}_{-46}	17	13	0.38±0.17	25
G1_1103[a]	0.6258	329^{+50}_{-28}	14	10	0.50±0.22	43
G1_1040.....	0.7798	259^{+91}_{-52}	8	6	0.83±0.37	32
G1_105411.....	0.6130	227^{+72}_{-28}	8	7	1.00±0.38	25
G1_105412.....	0.7305	182^{+58}_{-69}	10	10	0.50±0.22	7
G2_1040.....	0.6316	179^{+40}_{-26}	11	8	1.00±0.35	31

NOTES.—Col. (1): Name of the structure. Col. (2): Redshift. Col. (3): Velocity dispersion. Col. (4): Number of spectroscopically confirmed members. Col. (5): Number of galaxy members of the cluster used for the calculation of the O II fraction and hence brighter than the adopted magnitude limit. Col. (6): O II fraction. Col. (7): Distance from another structure in units of σ of the most massive of the two.

[a] Named Cl 1103.7−1245a in White et al. (2005).

5.3. *Other Environments at High z*

About 35% of the galaxies in the EDisCS spectroscopic catalog reside in the 18 structures that have been discussed so far. The other spectra can be used to investigate other environments at high redshift, such as groups and the "field."

We have identified other structures in our spectroscopic sample as associations in redshift space. Given our selection criteria for spectroscopic targets (§ 2 and Halliday et al. 2004), we can treat the spectroscopic catalog in a redshift slice close to the redshift targeted in each field as a purely *I*-band–selected sample (B. Milvang-Jensen et al. 2006, in preparation). To ensure that no selection bias can be present, we choose conservative redshift limits and only consider galaxies within ± 0.1 in z from the cluster targeted in each field. With these criteria we can study two other clusters ($\sigma > 400$ km s^{-1}), listed in Table 5, and several groups ($\sigma < 400$ km s^{-1}).

[25] We note that this is done selecting halos at $z = 0$ and computing the average projected velocity dispersion of their "main progenitor" at $z = 0.6$. We have verified that selecting halos at $z = 0.6$ and following their descendants to $z = 0$ gives similar results, albeit the amount of evolution in σ turns out to be slightly smaller in this case. The differences found with the two selection methods increase with the halo velocity dispersion ranging from less than 10 km s^{-1} for systems up to 500 km s^{-1} to about 100 km s^{-1} for systems with 1000 km s^{-1}.

[26] We stress that Table 4 extends to lower and higher masses than those probed by our sample at low redshift. Therefore, for systems with σ below 350 and above 1000 km s^{-1} at $z = 0$ the values listed are *extrapolations* of the observed trends, not confirmed by any observational evidence. According to these extrapolations, no change in O II fraction with redshift would be observed for systems below 200 km s^{-1}. At these low masses also the evolution of σ (mass) is negligible (Table 4).

[27] It is worth noting that the star-forming fractions in clusters with $\sigma > 1000$ km s^{-1} on average are quite similar at $z = 0.6$ and 0 (compare the left panel in Fig. 4 with the right panel in the same figure and with Fig. 6). However, as shown in Fig. 7 and Table 4, clusters with $\sigma > 1000$ km s^{-1} at $z = 0$ are those whose mass evolved the most between the two redshifts. Their progenitors at $z = 0.6$ were $\sim$800 km s^{-1} systems, whose star-forming fraction was higher than that of their descendants at $z = 0$. Thus, also the most massive systems at $z = 0$ on average have experienced a significant evolution of their fraction of star-forming galaxies.

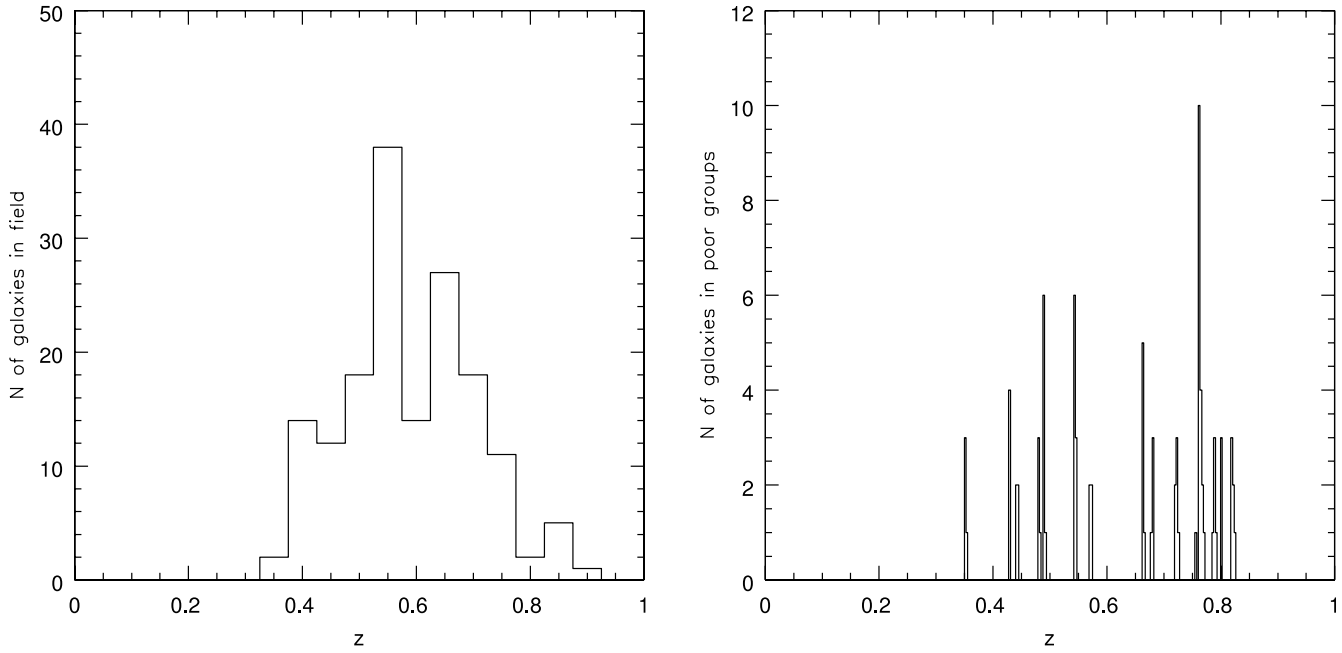

FIG. 9.—*Left*: Redshift distribution of our field spectroscopic sample. *Right*: Redshift distribution of galaxies in our poor groups.

Two types of groups have been isolated. Six structures have at least seven member galaxies with spectroscopic redshifts. For these, velocity dispersions have been computed. In the following we refer to these as "groups." These are listed in Table 5 and are among the groups studied in detail in a future paper.

Associations in redshift space with between three and six galaxies in our spectroscopic catalog have been treated separately and hereafter are referred to as "poor groups." In total our poor groups comprise 84 galaxies, whose redshift distribution is shown in Figure 9. We did not attempt to derive velocity dispersions for these systems given the small number of redshifts.

Any other galaxy in our spectroscopic catalog that was not a member of any of our clusters, groups, or poor group associations is hereafter named a "field" galaxy. Our field sample is composed of 162 galaxies, whose redshift distribution is shown in Figure 9. Our field sample should be dominated by galaxies in regions less populated than the clusters/groups/poor groups we isolated but will also contain galaxies belonging to structures that were not detected in our spectroscopic catalog.

The O II fractions in these additional structures and in the field have been computed for galaxies with absolute magnitudes brighter than the limit adopted for the main 18 structures described in § 3. No radial distance criterion has been introduced for the additional structures (those presented in Table 5 and the poor groups) and the field. The lack of a radial criterion, however, does not significantly affect the O II fractions derived for these systems.

The fraction of O II emitters we find in the "field" is $f_{[O\,II]} = 0.74$ and is shown in Figure 10 as a solid horizontal line with its error bars. The O II fraction in poor groups is even higher (87%; Fig. 10, dashed horizontal line), although still compatible with the fraction in the field within the errors.

The other structures for which we derived a velocity dispersion are shown in Figure 10 as open triangles. Among these, there are four systems with very high O II fractions ranging between 83% and 100%. In redshift space, these systems are all far from any known cluster, always at least $17\sigma_{clu}$ away (see Table 5). The other four additional structures in Figure 10 have relatively low O II fractions, around 40%–50%. Two of these are quite close to other massive structures ($7\sigma_{clu}$ from the most massive cluster in that field; see Table 5).

To summarize, both the field and the poor groups contain a high proportion of star-forming galaxies (70%–100%), comparable to that observed in more than half of the systems with $\sigma < 400$ km s^{-1}, and in agreement with the line that traces the relation between $f_{[O\,II]}$ and σ up to the most massive systems. In addition, there are five other groups with $\sigma < 400$ km s^{-1} (including Cl 1119 and Cl 1420, previously discussed) that have O II fractions

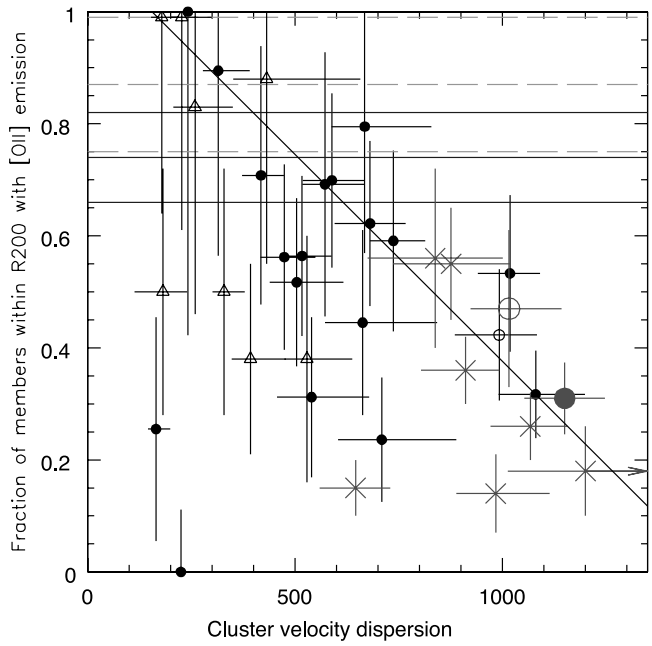

FIG. 10.—Same as Fig. 4, but now including also other environments. Open triangles are other EDisCS structures with at least seven spectroscopically confirmed members as in Table 5. The average O II fraction and corresponding error bars in poor groups (those between three and six spectroscopic members) are shown with dashed lines. The O II fraction among field galaxies (see text) and its error bars are shown as solid lines. [*See the electronic edition of the Journal for a color version of this figure*.]

significantly lower than the rest of the groups and the field. Their O II fractions are $\leq$50%. We come back to discussing these systems and describe their properties and those of their galaxy populations in § 5.5.

5.4. EW([O II]) *Distributions*

As shown above, the fraction of star-forming galaxies in high-redshift clusters depends on cluster velocity dispersion. It is interesting to investigate whether also the star formation activity in star-forming galaxies depends on σ and, more generally, on environment. In this section we analyze how the distributions of EW([O II]) for star-forming EDisCS galaxies vary in the different environments. We do not attempt any comparison with the low-redshift sample, given that a quantitative comparison of the EW strength is affected by the uncertainties related to aperture effects between $z = 0.8$ and 0.

We consider the "environments" defined in § 5.3, namely, clusters, groups, poor groups, and field. Clusters have been further subdivided into more and less massive clusters. We define as "massive clusters" all clusters in Table 1 with $\sigma > 800$ km s^{-1} (Cl 1216, Cl 1232) and as "less massive clusters" those with 400 km s^{-1} $< \sigma <$ 800 km s^{-1} (Cl 1138, Cl 1411, Cl 1301, Cl 1354, Cl 1353, Cl 1054−11, Cl 1227, Cl 1202, Cl 1059, Cl 1054−12, Cl 1018, Cl 1040). Among the groups, we consider separately groups with high and low O II fractions as discussed in the previous section. "Groups with low emission" are those groups with $\sigma < 400$ km s^{-1} and O II fractions significantly below the line in Figure 4 (Cl 1420, Cl 1119, G1_105412, G1_1301, G1_1103). "Groups with high emission" are those groups with $\sigma < 400$ km s^{-1} and O II fractions that roughly follow the line in Figure 4 (Cl 1037, Cl 1103, G1_1040, G2_1040, G1_1054−11). The same radial, magnitude, and EW limits and completeness weights used for computing the O II fractions have been applied to the EW distributions.

We have studied the proportion of star-forming galaxies with strong (EW < -40 Å), intermediate (-40 Å $<$ EW < -20 Å), and relatively modest equivalent width of (O II) (-20 Å $<$ EW < -3 Å).[28] These proportions are shown in Figure 11 as a function of environment. When ordering the environments in order of decreasing O II fraction, there is a progressive trend also in equivalent width strength. The fraction of galaxies with relatively weak EW (-20 Å $<$ EW < -3 Å; *circles*) decreases going to environments with higher O II fraction. The fraction of galaxies with intermediate-strength EW (*triangles*) follows the opposite trend. The fraction of galaxies with strong EW (EW $<$ -40 Å; *crosses*) appears higher in the field than in any other environment, and a possible excess is observed in massive clusters compared to the other environments.[29] These trends are visible in both the completeness-weighted and unweighted distributions (Fig. 11, *filled and open symbols*), except for the fraction of galaxies with strong EWs in the field that is significantly reduced when the completeness correction is ignored. The minimum error bar for each point in Figure 11 is computed from Poissonian statistics, while total error bars have been increased to take into account the difference between weighted and unweighted values. Total error bars are plotted in Figure 11.

[28] Note that the equivalent width measures the strength of the O II line relative to the underlying continuum. As such, it is not proportional to the star formation rate in solar masses per year, but to the current star formation rate per unit of galaxy luminosity at ~3700 Å.

[29] The presence of some galaxies with very high EWs in massive clusters is consistent with the detection of some spiral galaxies with enhanced star formation in rich clusters (see, e.g., Milvang-Jensen et al. 2003; Bamford et al. 2005 and references therein).

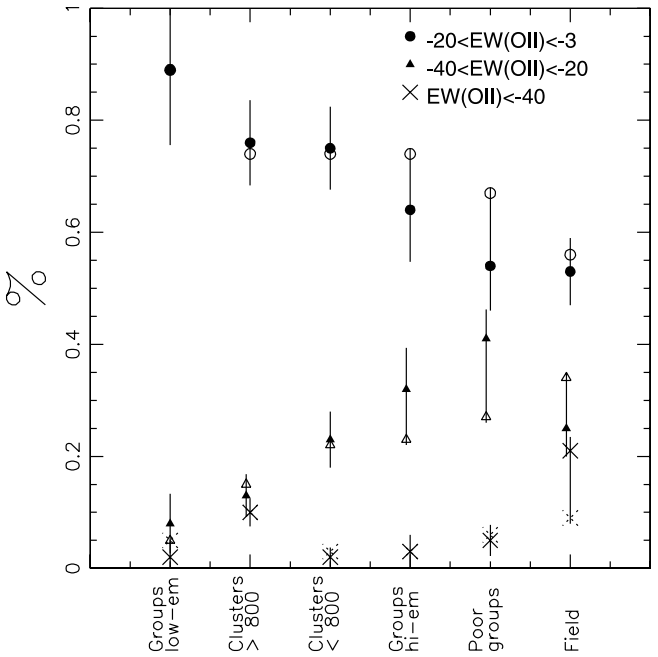

FIG. 11.—Fraction of star-forming galaxies with a strong, moderate, and relatively weak equivalent width of O II in different environments. Environments are located on the *x*-axis in order of increasing average O II fraction as from Fig. 4. The fraction of galaxies with relatively low EW (-20 Å $<$ EW $<$ -3 Å; *circles*) decreases going to environments with higher O II fraction. The fraction of galaxies with intermediate-strength EW (*triangles*) follows the opposite trend. The fraction of galaxies with strong EW (EW < -40 Å; *crosses*) is higher in the field than in any other environment, and a possible excess is observed in massive clusters compared to the other environments. Filled symbols and solid crosses refer to values corrected for incompleteness, while the uncorrected values are shown as open symbols and dashed crosses.

Thus, it is not only the proportion of galaxies with active star formation that changes as a function of environment, but also the star formation properties in star-forming galaxies. The two things are closely related to each other, following a parallel progressive trend: the distribution of EW(O II) is more skewed toward high values for environments with higher O II fractions. This seems to be at odds with the uniformity of the EW(Hα) distribution as a function of environment found by Balogh et al. (2004) for local samples, although a study analogous to ours has not been carried out at low *z*.

In principle, a different EW distribution could simply reflect a different luminosity distribution of galaxies in the different environments, since lower luminosity star-forming galaxies are known to have on average higher EWs than bright star-forming galaxies. To investigate whether the differences in the EW(O II) distributions are due to a different luminosity distribution with environment, or whether it is the star formation in galaxies of similar luminosity that changes with environment, we plot in Figure 12 the number density distribution of star-forming galaxies in a two-dimensional space of galaxy absolute *V* magnitude and EW(O II).

Following a well-known trend, galaxies occupy a characteristic triangular region in this diagram: in all environments, there are no or at most a few bright galaxies with EW(O II) stronger than -20 Å, while going to fainter magnitudes the EW distribution extends to stronger and stronger EWs. In fact, fainter galaxies span a wide range of EWs, while the brightest galaxies are confined to small/moderate EWs.

While these are the general trends, the maps also show some interesting variations with environment. Groups with low O II

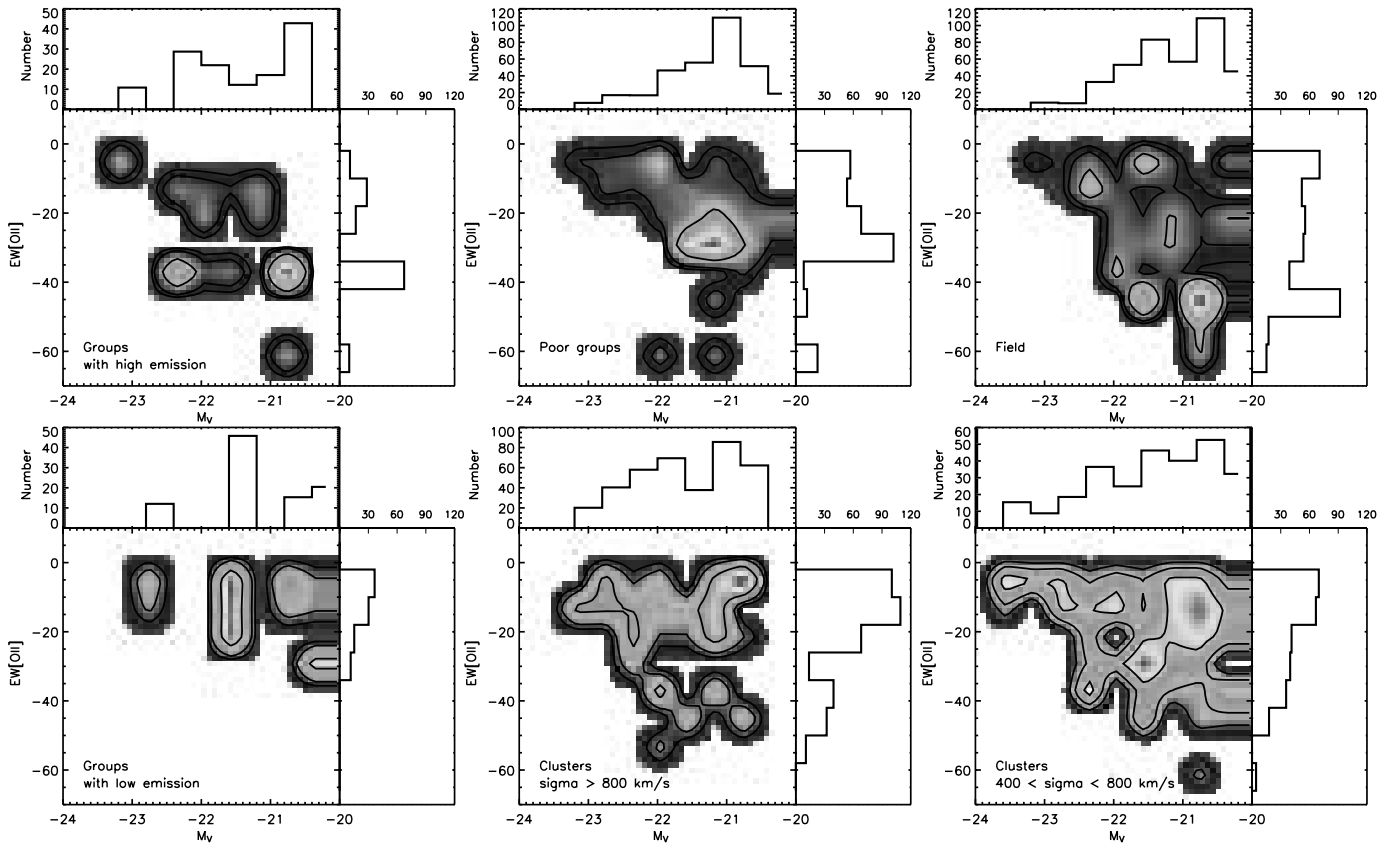

FIG. 12.—Number density maps of star-forming galaxies in different environments as a function of galaxy absolute V magnitude and EW(O II). Contours represent 25th, 75th, and 90th percentiles, while the gray scale is meant to guide the eye. The histograms on top and on the right present the number of galaxies in bins of absolute magnitude and EW(O II), respectively. Numbers in this figure have been corrected for spectroscopic incompleteness. The raw (uncorrected) numbers of galaxies are 39 (massive clusters), 126 (less massive clusters), 31 (groups with high emission), 19 (groups with low emission), 51 (poor groups), and 75 (field). [*See the electronic edition of the Journal for a color version of this figure.*]

fractions (*bottom left panel*) lack a significant population of faint galaxies with moderate and strong EWs that *are* present in the other environments. In these groups, star-forming galaxies have weak EWs, regardless of their luminosity. According to a K-S test, considering only star-forming galaxies with $M_V = -20$ to -21.5, the EW distribution in groups with low O II emission is different from the summed distribution in all other environments at the 99.9% confidence level (99.4% if the EW distributions are not weighted for completeness).

Inspecting the histograms of EW(O II) (on the right side of each panel), the field and poor group environments (*top middle and top right panels*) display an excess of galaxies with intermediate and strong EWs compared to both massive and less massive clusters (*bottom middle and bottom right panels*). This is the same effect seen in Figure 11, which shows that the fraction of galaxies with intermediate+strong EWs increases going from clusters to poor groups and the field. The distributions of absolute magnitudes of star-forming galaxies are presented in the top histogram of each panel. These show that the magnitude distribution in the field and poor groups is skewed toward fainter average magnitudes than in clusters of all masses. In fact, the absolute magnitude distribution in the field+poor groups differs from that in clusters at the 99.9% confidence level. In this case, the difference is not significant if the distributions are unweighted. Moreover, at a given faint luminosity, galaxies in the field and poor groups tend to have stronger EWs on average than similarly luminous star-forming galaxies in clusters (see the variation of the Y position of the red/yellow highest peak at faint magnitudes in the maps of field/poor groups vs. clusters). The difference in the EW distribution for faint galaxies ($M_V = -20$ to -21.5) in field+poor groups compared to massive+less massive clusters is significant at the 99.9% level (96.0% if unweighted).

Thus, the behavior of the EW(O II) distributions with environment seen in Figure 11 appears to be the result of a combination of different EWs at a given faint luminosity (stronger EWs in environments with higher star-forming fractions) and different luminosity distributions of star-forming galaxies (a higher faint-to-bright galaxy number ratio in environments with higher star-forming fractions).

5.5. *Outliers in the* O II–σ *Relation*

It is worth analyzing separately the properties of outliers from the O II–σ relation. Here we consider as outliers those EDisCS structures with an O II fraction significantly lower than the fractions of the majority of structures of similar velocity dispersion.

The two most outstanding outliers are two groups, Cl 1119 and Cl 1420, with $\sigma = 165$ and 225 km s^{-1}, respectively, and an O II fraction <30%. Both of these structures have quite a high number of spectroscopically confirmed bright members (>20) within a small velocity dispersion. For Cl 1119, the nondetection in the weak-lensing analysis and the corresponding upper limit on σ confirm the low-mass nature of this system, while for Cl 1420 a meaningful comparison cannot be performed because the lensing-based estimate is likely contaminated by other mass structures (Clowe et al. 2006). Thus, at least for Cl 1119 this seems to rule out the possibility that the system deviates from the general

trend due to its σ measurement strongly underestimating its mass. Moreover, as shown in column (12) of Table 1, these two systems remain outliers also if we relax the R_{200} criterion and compute the O II fraction over a larger field.[30]

Interestingly, besides the low O II fractions, these two systems also stand out for their unusually high fraction of early-type galaxies for their velocity dispersion, as found by the analysis of galaxy structural parameters based on two-dimensional bulge+disk decomposition (L. Simard et al. 2006, in preparation), and for their low fractions of blue galaxies (G. De Lucia et al. 2006, in preparation). The evidence for the peculiarity of these outliers is further reinforced by the analysis of the O II equivalent width distributions. We have seen in § 5.4 that the EW distribution in star-forming galaxies of the groups with low O II fractions (including Cl 1119 and C 1420) is different from that in any other environment. The population of faint galaxies with strong EWs, common in other environments, is absent in these groups. All of these findings (low O II and blue fractions, high early-type fractions for their velocity dispersion, as well as peculiar equivalent width distribution of O II) suggest that these groups are intrinsically peculiar when compared to the majority of other structures. In fact, the properties of their galaxies resemble those of galaxies in the core of much more massive clusters, as if they were "bare" massive-cluster cores lacking the less centrally concentrated population of star-forming galaxies.

Another point worth stressing concerns those systems that are relatively close in redshift to a cluster (within $10\sigma_{\rm clu}$) without being part of it (at velocities $>3\sigma_{\rm clu}$). There are two such systems in our sample, G1_105412 and C2_1138 in Table 5. Both of these systems have a low star-forming fraction for their velocity dispersion. An intriguing hypothesis is that systems close to more massive structures, thus embedded in a massive superstructure, have a different galactic content than completely isolated systems of similar mass. On the other hand, the two other groups with a low O II fraction (G1_1301 and G1_1103) are much farther away from any other structure detected within the field we observed (26 and 47 σ, respectively).

The O II–σ trend observed at high redshift is suggesting that the fraction of star-forming galaxies in clusters 5–7 Gyr ago depends on cluster mass, or on something that is closely related to the cluster mass. The existence and characteristics of the outliers, as well as the fact that the two systems close to other structures possess a low O II fraction, seem to suggest that the driving factor might be density (mass per unit volume), instead of mass.[31] Density and mass will be closely related for most systems, and the outliers might be those systems of unusually high density for their mass, i.e., those regions that were very dense at high redshift but failed to acquire star-forming galaxies at later times, possibly due to the characteristics of their surrounding supercluster environment.

5.6. *Star Formation versus Galaxy Morphologies*

As shown in § 5.2, the relation between the O II fraction and the cluster velocity dispersion changes significantly between $z = 0.8$ and 0. Over the same redshift range, also galaxy morphologies have been observed to evolve in clusters. Distant clusters generally contain a higher proportion of spiral galaxies, and a correspondingly lower proportion of S0 galaxies, than low-z clusters (Dressler et al. 1997; Couch et al. 1998; Fasano et al. 2000; Treu et al. 2003; Smith et al. 2005; Postman et al. 2005). Low S0 fractions and high spiral fractions are found also in our sample, and we refer to V. Desai et al. (2006, in preparation) and L. Simard et al. (2006, in preparation) for a detailed analysis of the morphological content of EDisCS clusters. It is then interesting to investigate whether galaxy morphologies evolve with redshift in the same way as the star-forming fraction does, as well as how the star formation histories of galaxies are related to the Hubble type.

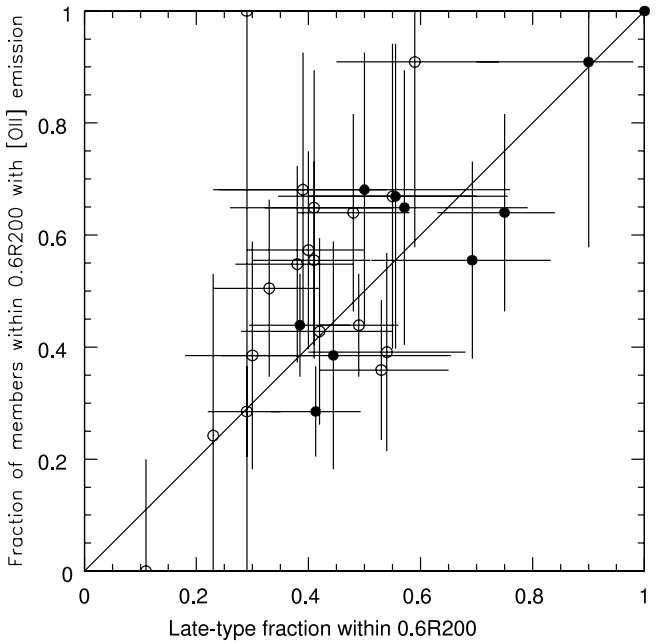

FIG. 13.—O II fraction of EDisCS clusters vs. the fraction of late-type galaxies, both computed within $0.6R_{200}$ and down to $M_V = -20.0$. The late-type fraction is computed as the fraction of spectroscopically confirmed members. Open circles represent the fraction of late-type galaxies obtained from structural parameters derived from two-dimensional bulge+disk decompositions of VLT images (L. Simard et al. 2006, in preparation). Filled circles represent the fraction of late-type galaxies (all galaxies excluding elliptical and S0 galaxies) derived from visual morphological classifications of *HST* images (V. Desai et al. 2006, in preparation). The 1 : 1 line is shown for comparison.

Figure 13 presents the O II fraction versus the fraction of late-type galaxies (spiral+irregular) for EDisCS clusters. The fraction of late-type galaxies has been derived with two different methods: for clusters with *HST* imaging, from visual morphological classifications (V. Desai et al. 2006, in preparation), and for all 18 systems using structural parameters derived from two-dimensional bulge+disk decompositions of VLT images (L. Simard et al. 2006, in preparation). A comparison of visual and automated classifications can be found in L. Simard et al. (2006, in preparation). The plot shows that the proportions of late-type galaxies are roughly consistent with the star-forming fractions we find in this paper. We note, for example, that the two systems with the lowest O II fractions (Cl 1119 and Cl 1420) are also those with the lowest late-type fractions.

We now compare the evolution of the star-forming fraction with the evolution of the morphological types. In massive clusters ($\sigma = 800$–1100 km s^{-1}) the fraction of late-type galaxies evolves from 30%–50% at high z to $\sim$20% at $z = 0$ (V. Desai et al. 2006, in preparation; Fasano et al. 2000).[32] This corresponds to a comparable increase of the S0 galaxy fraction. For clusters of this velocity dispersion we find that the star-forming fraction

[30] The O II fraction of Cl 1420 changes from 0% within R_{200} to 40% over the whole FORS2 field. Even adopting the latter value, however, this system remains an outlier for its velocity dispersion.

[31] Interestingly, as shown by Gray et al. (2004) for the Abell 901/902 supercluster, the local dark matter mass density measured from weak gravitational lensing correlates with local galaxy number density, although with considerable scatter.

[32] The late-type fractions are computed for galaxies brighter than $M_V = -20.7$.

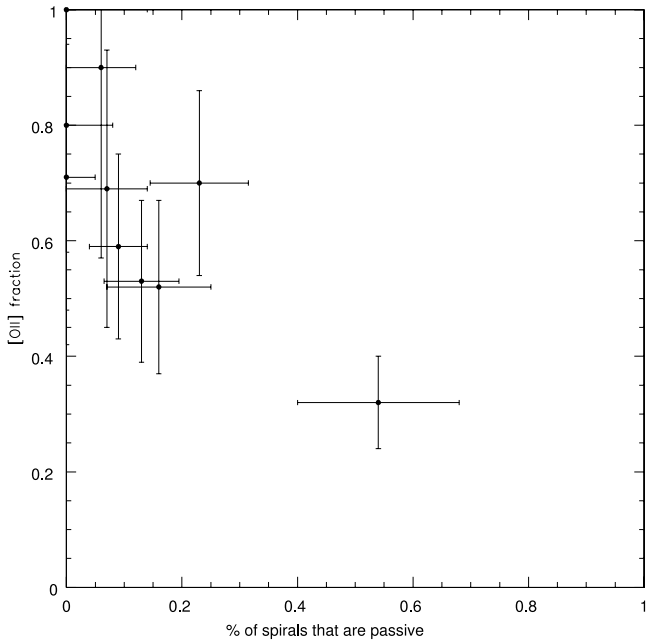

FIG. 14.—Fraction of late-type galaxies (spiral+irregular galaxies from *HST* images) that are passive (lack emission lines in their spectra) vs. O II fraction for EDisCS systems.

changes on average from 30%–50% at $z = 0.6$ to 20% at $z = 0$ (Fig. 4). In massive clusters, the change in the star-forming fraction is therefore similar to the observed evolution of the late-type population.

In clusters with $\sigma = 400-700$ km s^{-1}, both the late-type and the star-forming fractions range from about 40% to 80% at high redshift (V. Desai et al. 2006, in preparation; this paper). Unfortunately, a detailed study of the elliptical/S0/spiral fractions as a function of the cluster velocity dispersion is not available at low redshift for comparison. If the evolution of the star-forming fraction between $z = 0.6$ and 0 reflects the evolution of spiral galaxies into S0 galaxies (and vice versa), our results on the O II evolution as a function of the system mass would imply that the evolution of the S0 population should be maximum in intermediate-mass clusters, those with $\sim$600 km s^{-1} at $z = 0$.

The agreement between the evolution of the star-forming and S0 fractions suggests that star-forming late-type galaxies are being transformed into passive S0 galaxies. However, it is necessary to stress that morphology and star formation history can be partly decoupled in clusters: several of the cluster spiral galaxies at all redshifts do not have emission lines in their spectra, and both their spectra and their colors indicate a lack of current star formation activity (e.g., Poggianti et al. 1999; Couch et al. 2001; Goto et al. 2003). These passive spiral galaxies are believed to be an intermediate stage in the transformation from star-forming spiral galaxies to passive S0 galaxies. The existence of passive spiral galaxies and the fact that most of the poststarburst galaxies in distant clusters have spiral morphologies (Dressler et al. 1999; Poggianti et al. 1999) are strong indications that the timescale for morphological transformation is longer than the timescale over which the spectrophotometric signature of recent star formation disappears: galaxies are first quenched, and then eventually their morphology changes on a longer average timescale (Poggianti et al. 1999).

Also in EDisCS clusters the populations of star-forming (i.e., emission line) and late-type galaxies do not fully coincide. On average over all clusters, we find that 15% of the star-forming galaxies are classified as elliptical or S0 galaxies and conversely that 13% of the morphologically late-type galaxies do not show any sign of ongoing star formation. A detailed one-to-one comparison between galaxy morphologies and star formation histories in EDisCS clusters is deferred to a later paper, but for the purposes of this paper we plot the fraction of spiral galaxies that are passive versus the O II fractions in Figure 14. There is a hint that clusters with a lower O II fraction also might have a higher proportion of their spiral galaxies that are passive, although this conclusion is mostly based on one cluster (Cl 1232) in which >50% of the spiral galaxies are passive.

The decoupling of morphologies and star formation, however, involves only a relatively modest proportion of galaxies in most clusters. In addition, those clusters with the highest fraction of spiral galaxies that are passive also tend to be those with the lowest fraction of spiral galaxies; therefore, the decoupling is not strongly affecting the global morphological budget. It remains true that the correspondence between the morphological evolution and the evolution in the star-forming fraction supports the hypothesis that the evolution observed between $z = 0.8$ and 0 concerns star-forming late-type galaxies evolving into passive S0 galaxies.

6. DISCUSSION

The results found in this paper provide for the first time a quantitative description of the evolution of the star-forming galaxy population in clusters as a function of redshift and σ. These results highlight the need to study the evolution of the star-forming galaxy fraction as a function of system mass. Ignoring this dependence can lead to incorrect conclusions regarding the evolution. Low-z surveys lack large numbers of massive clusters with $\sigma \geq 1000$ km s^{-1} (due to their rarity), while most high-z samples include only the most massive clusters. If the cluster mass dependence is not taken into account, 1000 km s^{-1} high-z clusters end up being compared with 500–700 km s^{-1} low-z clusters, making the evolution harder to detect.

Our results also provide a likely explanation of why it has been so difficult to observe trends with cluster mass/σ. The way the data are distributed in Figure 4 already shows that finding the general trends of star-forming fraction with system mass requires (1) a large number of clusters, with data as homogeneous as possible; (2) a sample covering a wide range of cluster masses; (3) a high-quality spectroscopic data set, in terms of both the number of spectra per cluster and the quality of the spectra themselves; and (4) reliable and thoroughly controlled σ-values when using velocity dispersion as a proxy for mass. The most crucial requirement is the range of cluster/group masses that needs to be explored. For example, from Figure 4 it is evident that sampling at high z only half of the range in σ (only systems with $\sigma > 700$ km s^{-1} or $\sigma < 700$ km s^{-1}) would result in the trend being buried in the scatter and unrecognizable. At low z, no trend can be observed when including only systems with $\sigma > 500$ km s^{-1}.

This might explain at least some of the contrasting results that have been found in the literature regarding the presence or absence of a relation between galaxy properties and system "mass" as determined from velocity dispersion, X-ray luminosity, or other global cluster properties. For example, the relatively limited range in cluster mass explored by X-ray-selected samples might be the reason why several works could not find a trend of blue fraction with cluster X-ray luminosity (Smail et al. 1998; Andreon & Ettori 1999; Ellingson et al. 2001; Fairley et al. 2002). Only sampling the whole mass range, from groups to massive clusters, trends at high and low z become recognizable. In this respect, the fact that the mass distribution of EDisCS clusters differs significantly from the distribution of X-ray–selected samples at high redshift, extending

to much lower masses (Clowe et al. 2006), is an advantage. Moreover, the range of masses sampled by EDisCS, when evolved to $z = 0$, matches significantly better the mass distribution of nearby clusters than X-ray high-z samples do, as the latter only contain the progenitors of the highest mass tip of the low-redshift cluster mass distribution. It is also true that very low mass/low richness noncentrally concentrated systems could be underrepresented in our sample, given the selection method of EDisCS. These types of systems are generally those with the highest incidence of star-forming galaxies. Hence, although our selection criteria could not be responsible for the O II–σ trend observed, they might influence the observed density of points in the O II–σ diagram. If anything, there should be more high–O II low-mass groups and the O II–σ relation would then be even stronger than we have observed.

6.1. *A Possible Scenario for the Trends of the Star Formation Activity as a Function of Environment*

Understanding the origin of the trends of star formation with velocity dispersion would represent a significant step forward toward comprehending the link between galaxy evolution and environment. If galaxy properties depend on the mass of the system where they reside or have resided during their evolution, there should be a connection between the trends observed and the way cosmological structures have grown in mass with redshift.

In this section we investigate whether the trends in star formation activity correspond in some way to the growth history of structure. To quantify the evolution of cosmological structures, we adopt two different approaches. Using a Press-Schechter (PS) formalism (Bower 1991; Lacey & Cole 1993), we analyze the growth history of systems of different mass. In particular, we study what fraction of the system mass was already in massive structures at different redshifts. In addition, we use the Millennium Simulation (Springel et al. 2005) to study the growth history in terms of number fraction of galaxies instead of mass, to assess what fraction of the galaxies in systems of a given mass were already in massive structures at different redshifts. This was computed by populating dark matter halos with galaxies by means of semianalytic models (De Lucia et al. 2006; Croton et al. 2006). We have chosen to employ both approaches because it is important to examine the results in terms of both mass and number of galaxies. The evolution of the mass of cosmological structures is totally independent of assumptions regarding galaxy formation and evolution; therefore, it is not affected by all of the uncertainties inherent to these assumptions. At the same time, it is important to ascertain whether the evolution in the number of galaxies follows the mass evolution, given that the former quantity is the one that is directly observed.

In the following we name "clusters" systems with masses $>10^{14}\ M_{\odot}$ and "groups" systems with masses between $3 \times 10^{12}\ M_{\odot} < M < 10^{14}\ M_{\odot}$. These mass limits approximately correspond to the velocity dispersion limits we have adopted in this paper for defining clusters and groups (>400 and <400 km s^{-1}, respectively).

In the comparison between observations and theory we are guided by four considerations:

1. So far, we have focused on the fraction of star-forming galaxies $f_{[\mathrm{O\,II}]}$. At each epoch and in each environment, the fraction of galaxies with no ongoing star formation is simply $(1 - f_{[\mathrm{O\,II}]})$, and we refer to these as "passive galaxies." Observational studies of clusters suggest that there may be two distinct families of passive galaxies:

   (*a*) The first family is composed of galaxies whose stars all formed at very high redshift ($z > 2$) over a short timescale, which have been observed in clusters up to and beyond $z = 1$ (Bower et al. 1992; Ellis et al. 1997; Barger et al. 1998; Kodama et al. 1998; van Dokkum et al. 2000, 2001; Blakeslee et al. 2003; De Lucia et al. 2004; Barrientos et al. 2004; Holden et al. 2005). This family is largely composed of luminous cluster elliptical galaxies (e.g., Ellis et al. 1997).

   (*b*) The second family corresponds to passive galaxies that have had a more extended period of star formation activity (with a longer star formation timescale). Star formation in these galaxies has been quenched when they were accreted into the dense environment (Dressler & Gunn 1983, 1992; Couch & Sharples 1987; Balogh et al. 1997; Poggianti et al. 1999; Ellingson et al. 2001; Kodama & Bower 2001; van Dokkum & Franx 2001; Tran et al. 2003; Poggianti et al. 2004; Wilman et al. 2005b). Most of these galaxies are spiral galaxies up to at least 1 Gyr after the star formation is quenched (Dressler et al. 1999; Poggianti et al. 1999; Tran et al. 2003). The passive nature of these galaxies is considered to be a consequence of the interaction with their environment.

In the following we refer to these two families as "primordial passive galaxies" and "quenched galaxies," respectively. As the growth of cosmological structures proceeds and clusters and groups accrete more galaxies, we should expect the relative proportion of the two types of passive galaxies to change. In those environments that efficiently quench star formation, quenched galaxies should progressively become a larger part of the passive population (going to lower redshifts), while primordial passive galaxies should dominate the passive population in systems at high redshift.

2. Observationally, primordial passive galaxies are preferentially located in the densest, more massive structures at all redshifts. At the epoch when they formed their stars ($z \geq 2.5$), essentially no system more massive than $10^{14}\ M_{\odot}$ existed according to current hierarchical theories. The most massive structures at $z = 2.5$ had masses similar to those of systems that at low redshift we would call "groups" ($>3 \times 10^{12}$). Thus, when they had just completed their star formation, primordial passive galaxies were in systems of masses comparable to groups today.

3. Considering cluster crossing times (typically 1 Gyr), timescales associated with the various physical processes that might lead to the truncation of the star formation activity (e.g., harassment, ram pressure, strangulation, mergers; 1–2 Gyr at most), and the spectrophometric timescale for the evolution of the O II signature ($\sim 5 \times 10^7$ yr), a few billion years should be sufficient for suppressing the O II emission in most quenched galaxies. We consider then a timescale of 3 Gyr as a reasonable upper limit for the time required to totally extinguish star formation in newly accreted galaxies.

4. The existence of a break point ($\sim$550 km s^{-1}) in the O II–σ relation observed at low redshift, above which essentially every system has a low O II fraction regardless of its mass, suggests that systems above this mass are highly efficient at quenching star formation in galaxies falling into them. A system with a velocity dispersion around $\sim$500 km s^{-1} at $z = 0$ approximately corresponds to a system that 3 Gyr ago (see point 3) had a mass $\sim(1-2) \times 10^{14}\ M_{\odot}$ (see Table 4). As a working hypothesis it is then natural to adopt $10^{14}\ M_{\odot}$ as the reference mass for efficiently quenching star formation, i.e., the mass above which the quenching is a widespread phenomenon affecting sooner or later (within 3 Gyr according to point 3) all accreted galaxies.

We first consider the family of primordial passive galaxies. In Figure 15 we compare the O II observations at $z = 0.4-0.8$ with the theoretical expectations for the growth history. The solid line (in both panels) is the line drawn in the O II–σ diagram observed

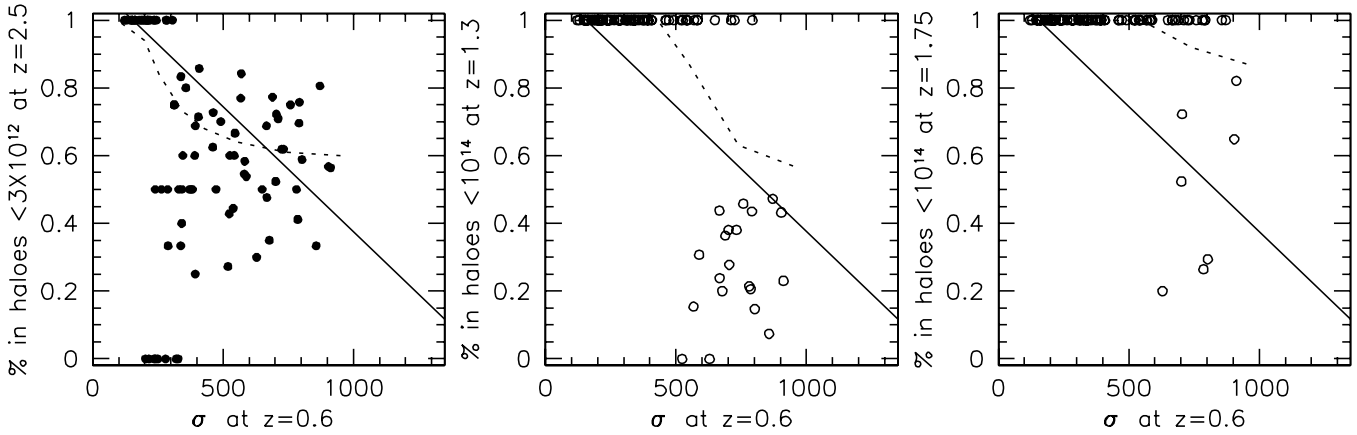

FIG. 15.—Clusters at high redshift. The solid line is the line drawn in the O II–σ diagram observed at high redshift. *Left*: Filled circles represent the fraction of galaxies in 90 halos selected at $z = 0.6$ in the MS simulation that were in halos with mass $<3 \times 10^{12}\ M_\odot$ at $z = 2.5$. The dashed line is the prediction of the average fraction of mass in halos $<3 \times 10^{12}\ M_\odot$ at $z = 2.5$ derived from the PS formalism. *Middle*: Open circles represent the fraction of galaxies in the MS simulation that were in halos with mass $<10^{14}\ M_\odot$ ~3 Gyr prior to $z = 0.6$, thus at $z = 1.3$. The dashed line is the prediction of the fraction of mass in halos $<10^{14}\ M_\odot$ at $z = 1.3$ derived from the PS. *Right*: Open circles represent the fraction of galaxies in the MS simulation that were in halos with mass $<10^{14}\ M_\odot$ ~3 Gyr prior to $z = 0.8$, thus at $z = 1.75$. The dashed line is the prediction of the fraction of mass in halos $<10^{14}\ M_\odot$ at $z = 1.75$ derived from the PS.

at $z = 0.4$–0.8 (Fig. 4). In the left panel, the dashed line is the fraction of mass of systems at $z = 0.6$ that was in systems with $M_{\rm sys} < 3 \times 10^{12}\ M_\odot$ at $z = 2.5$ as derived from the PS formalism, averaged over 100 halos. Filled circles represent the fraction of galaxies within R_{200} and with M_V limits as for EDisCS that were in systems with $M_{\rm sys} < 3 \times 10^{12}\ M_\odot$ at $z = 2.5$ obtained for 90 halos in the MS. Halos were in this case selected at $z = 0.6$ from the MS, similarly to how it was done for halos at $z = 0$ in § 5.2.

Both the PS results and the MS upper envelope trace remarkably well the O II–σ relation observed at high redshift. The scatter of the MS points illustrates that for systems of any given σ at $z \sim 0.6$ there is a range in the fraction of galaxies that were already in groups at $z = 2.5$. This scatter indeed resembles the scatter of the data points in the observed O II–σ diagram of distant clusters (see the left panel of Fig. 4). This figure shows that *the fraction of passive galaxies observed in* $z = 0.4$–0.8 *clusters of a given σ/mass is comparable with the fraction of its galaxies (or its mass) that was already in dense environments (i.e., groups) at* $z = 2.5$. We tentatively identify the latter with the population of primordial passive galaxies as described in point 2 above. Identifying primordial passive galaxies with galaxies already in groups at $z = 2.5$ implies that the great majority of galaxies belonging to environments more massive than $3 \times 10^{12}\ M_\odot$ at $z = 2.5$ completed their star formation activity at high redshift and, vice versa, that those galaxies that completed their star formation at high redshift are mostly galaxies that were in environments more massive than $3 \times 10^{12}\ M_\odot$ at $z = 2.5$.

We note that among the 90 halos extracted from the MS there are also a few "outliers" located in the lower left region of Figure 15. This means that a large fraction of their galaxies resided in halos of masses $M_{\rm sys} > 3 \times 10^{12}\ M_\odot$ at $z = 2.5$. The comparison between Figures 15 and 4 then suggests that O II outliers at high redshift might represent systems that had a high fraction of their mass already in groups at $z = 2.5$ and did not accrete a large population of field galaxies between $z = 2.5$ and ~0.6.

In the middle and right panels of Figure 15, we contrast the observed fractions of passive galaxies with the trends expected for quenched galaxies. Open circles in the middle panel show the fraction of galaxies in $z = 0.6$ systems in the MS that were in halos with mass $<10^{14}\ M_\odot$ ~3 Gyr prior to $z = 0.6$, thus at $z = 1.3$ (see points 3 and 4 above). For most systems with $\sigma <$ 700 km s^{-1} the fraction of galaxies that experienced the cluster environment for at least 3 Gyr is 0, and the predicted trend is inconsistent with the observational results. In these systems, the passive galaxy population is not consistent with the fraction of galaxies/mass that was already in systems more massive than $10^{14}\ M_\odot$ 3 Gyr prior to $z = 0.6$. In the most massive systems ($\sigma > 700$ km s^{-1}), the middle panel of Figure 15 shows that there is already a considerable fraction of galaxies at $z = 0.6$ that have resided in a cluster at least since $z = 1.3$. We find that only ~50% of these galaxies were in groups at $z = 2.5$; therefore, there is a nonnegligible proportion of galaxies that have experienced the cluster environment (i.e., have been quenched according to point 4) without being primordial passive galaxies. This suggests that, while the lower mass systems at $z = 0.6$ contain essentially no quenched galaxies, in more massive systems at these redshifts quenched galaxies can already account for more than $\frac{1}{3}$ of the passive population.

In the right panel of Figure 15, open circles show the fraction of galaxies in MS systems that were in halos with mass $<10^{14}\ M_\odot$ ~3 Gyr prior to $z = 0.8$ (the highest redshift in the sample we study here), thus at $z = 1.75$. Few galaxies have experienced prolonged exposure to cluster-like environments since $z = 1.75$. The comparison of the middle and right panels of Figure 15 shows that between $z = 1.75$ and 1.3 in massive systems there is a dramatic change in the fraction of mass/galaxies that have experienced environments more massive than $10^{14}\ M_\odot$; hence, $z \sim 1.5$ is an important epoch for the buildup of clusters and the beginning of the quenching process.

Turning to low redshifts, in Figure 16 we compare the trends observed in SDSS clusters (*solid line*) with the fraction of mass and galaxies in massive environments at previous redshifts. The left panel shows the fractions of mass and number of galaxies in systems at $z = 0$ that were in systems with $M_{\rm sys} < 3 \times 10^{12}\ M_\odot$ at $z = 2.5$ from the PS and MS (*dashed line and filled circles, respectively*). For the MS, only galaxies within R_{200} and with M_V limit as for SDSS are considered. *In contrast to the high-z clusters, the fraction of passive galaxies in systems at* $z = 0$ *does not agree well with the fraction of galaxies residing in groups already at high redshift. While 80% of galaxies in massive systems at* $z = 0$ *are passive, only 20% were in groups at* $z = 2.5$.

The right panel in Figure 16 shows the fractions of mass and galaxies that were in systems of mass $M_{\rm sys} < 10^{14}\ M_\odot$ 3 Gyr prior to the observations (corresponding to $z = 0.28$), from the

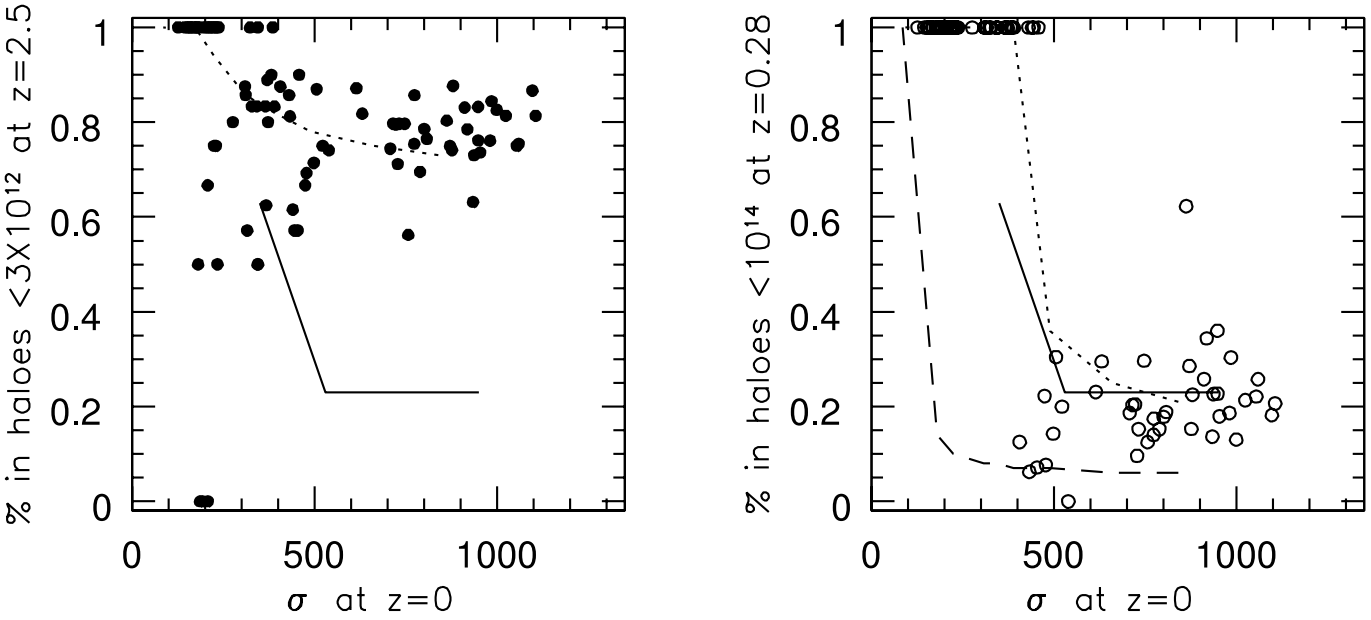

FIG. 16.—Clusters at low redshift. Comparison between the O II–σ relation observed at low redshift (*solid lines*) and results from the MS (*filled circles*) and from the PS formalism (*dashed lines*). *Left*: The solid lines trace the O II–σ relation observed at low redshift. Filled circles represent the fraction of galaxies in 90 halos in the MS simulation that were in halos with mass $<3 \times 10^{12}\ M_{\odot}$ at $z = 2.5$. The dashed line is the prediction of the fraction of mass in halos $<3 \times 10^{12}\ M_{\odot}$ at $z = 2.5$ for a system of a given σ at $z = 0.0$ derived from the PS formalism. *Right*: The solid lines are repeated from the left panel. Open circles represent the fraction of galaxies in 90 halos from the MS simulation that were in halos with mass $<10^{14}\ M_{\odot}$ ~3 Gyr prior to observations, thus at $z = 0.28$. The short-dashed line is the prediction of the fraction of mass in halos $<10^{14}\ M_{\odot}$ at $z = 0.28$ for a system of a given σ at $z = 0.0$ derived from the PS formalism. The long-dashed line is the prediction of the fraction of mass in halos $<3 \times 10^{12}\ M_{\odot}$ at $z = 0.28$ for a system of a given σ at $z = 0.0$ derived from the PS formalism.

PS and MS (*short-dashed line and open circles, respectively*). In this case, the agreement between the observations of SDSS clusters (*solid line*) and the PS and MS results is remarkable. This shows that *the observed fraction of passive galaxies in systems with* $\sigma > 500$ km s^{-1} *at* $z = 0$ *is compatible with the fraction of galaxies that have resided in a cluster* ($M_{\rm sys} > 10^{14}\ M_{\odot}$) *for at least 3 Gyr and therefore have had the time to have their star formation switched off* (see points 3 and 4 above). The passive population in clusters at $z = 0$ amounts to about 80% of all galaxies,[33] of which 20% (Fig. 16, *left panel*) are primordial passive galaxies that have evolved passively since $z = 2.5$ and 60% are galaxies that are quenched at lower redshift.[34] Also in this case the scatter in the growth history of MS halos is similar to the observed scatter in the fraction of star-forming galaxies (compare the right panels of Figs. 16 and 4). The scatter observed in the O II–σ relation at all redshifts probably simply reflects the scatter in the growth histories of systems of any given mass.

According to this discussion, while the passive galaxy populations of the distant clusters are predominantly composed of primordial passive galaxies, the populations of lower redshift clusters are dominated by quenched galaxies. We considered whether it is possible to obtain an agreement between the fraction of quenched galaxies and the high-z observations by choosing a lower reference mass for quenching star formation. However, the reference mass of $\sim 10^{14}\ M_{\odot}$ is set by the mass (3 Gyr ago) of a system with a velocity dispersion at $z = 0$ corresponding to the break observed at ~500 km s^{-1} in SDSS clusters. If the minimum mass of a system efficiently quenching star formation were much lower, such as, for example, $3 \times 10^{12}\ M_{\odot}$, the fraction of passive galaxies would be too high (and the fraction of star-forming galaxies too low) compared to the low-z observations, as shown by the long-dashed line in the right panel of Figure 16. Thus, under the assumption that physical processes operate at $z = 0.6$ as they do at $z = 0$ and adopting the same quenching reference mass at all redshifts, both the primordial and the quenched channels are required to simultaneously match the observed trends at high and low redshift.

A key point to note from this discussion is that the behavior of the O II fraction with σ at low redshift appears to rule out the possibility that the group environment universally quenches star formation. If the quenching was a widespread phenomenon in "groups" (systems with masses significantly lower than $\sim 10^{14}\ M_{\odot}$), then all groups and clusters at low redshift should contain much lower fractions of star-forming galaxies than is observed. We note that this does not exclude that star formation might be quenched in some galaxies in groups or all galaxies in some of the groups, but a truncation affecting all galaxies within 3 Gyr from infall into systems with masses $\ll 10^{14}\ M_{\odot}$ cannot be reconciled with the observations. Conversely, the $10^{14}\ M_{\odot}$ reference mass indicates that the quenching of the star formation is not limited to very massive clusters but is highly efficient also in low-mass clusters.

Adopting the scenario depicted above as our working hypothesis, we can address the questions raised in § 5.2:

1. Why does the proportion of passive/star-forming galaxies correlate/anticorrelate (with a large scatter) with the velocity dispersion of the system for the majority of clusters at $z = 0.4$–0.8? Our previous discussion shows that the observed fractions of passive galaxies at $z = 0.4$–0.8 roughly agree with the fraction of mass/galaxies that were already in groups at $z = 2.5$. Primordial passive galaxies make up most of the passive population observed at $z \sim 0.6$, but in systems more massive than 700 km s^{-1} the proportion of quenched galaxies is already significant. The

[33] Within R_{200} and for magnitudes brighter than $M_V = -19.8$.

[34] This is the case because we find that >90% of the galaxies that were in groups (halos with masses $M_{\rm sys} > 3 \times 10^{12}\ M_{\odot}$) at $z = 2.5$ end up being in clusters (halos with $M_{\rm sys} > 10^{14}\ M_{\odot}$) at $z = 0.28$. Thus, the population of galaxies in clusters at $z = 0.28$ (Fig. 16, *right panel*) essentially contains the galaxy population that was in groups at $z = 2.5$ (Fig. 16, *left panel*).

anticorrelation observed arises because more massive systems tend to have a higher fraction of their mass/galaxies that were already in groups at $z = 2.5$, and massive systems also have a significant population of quenched galaxies.

2. Why does the proportion of passive/star-forming galaxies evolve with redshift in the way observed? In other words, why is there a Butcher-Oemler effect? At any redshift, the star-forming population is made up of galaxies that were not in groups at $z > 2.5$ and were not in clusters in the last few billion years. In this scenario the proportion of star-forming galaxies varies with redshift because the proportion that was in groups at $z > 2.5$ and the proportion in clusters during the last 3 Gyr change according to the growth history, the sum of the two growing toward lower redshifts.

3. Why is there no clear trend with σ at $z = 0$ for systems more massive than 500 km s^{-1}? In clusters with $\sigma > 500$ km s^{-1} at $z = 0$, about 80% of all galaxies are passive and have resided in clusters for at least 3 Gyr. Of these, 20% are primordial passive galaxies that formed in groups at $z > 2.5$ and 60% are quenched galaxies. At $z = 0$, both the proportion of galaxies that were in groups at $z = 2.5$ and the proportion of galaxies that were quenched are flat as a function of the system mass, as shown by Figure 16, and this gives rise to the observed plateau at $\sigma >$ 500 km s^{-1}. In systems less massive than 400–500 km s^{-1}, which are not as efficient as more massive systems in quenching star formation in galaxies infalling into them, the passive population could in some cases still largely coincide with the population of primordial passive galaxies formed at $z > 2.5$. However, if all of the passive population in low-σ systems originated as primordial passive galaxies, systems at low z on average would have higher star-forming fractions than similar systems at high z (compare the left panels of Figs. 15 and 16). Hence, it is probable that either the same process active in clusters (but with a lower efficiency) and/or other mechanisms are at work suppressing star formation in some of the galaxies in groups, or in some of the groups. As discussed previously, if the most important factor were density instead of mass, the large scatter of the O II fractions at low σ could be due to variations of density for halos of similarly low masses. As discussed in the next section, the existence of S0 galaxies in groups may be suggesting that star formation is indeed truncated also in groups under certain circumstances.

The consistency between the observations and the theoretical scheme outlined above does not constitute a definite proof of the validity of this scenario; this should be further tested by additional observations, especially at redshifts even higher than those considered here. It is suggestive, however, to find that the observed star formation trends follow both qualitatively and quantitatively the growth history of structure. If the scenario we have proposed above approximates the real situation, its implications are far reaching, as discussed in the next section.

6.2. *Implications*

In the scenario outlined in the previous section there are two channels that "produce" passive galaxies in dense environments. Primordial passive galaxies form all of their stars at $z > 2$ and it is reasonable to largely identify them with elliptical galaxies, while quenched galaxies have their star formation truncated at much later times, when infalling into an environment that can cause a truncation in the star formation activity, and we tentatively identify them with the population of spiral galaxies evolving into S0 galaxies. Each one of these two channels seems to correspond to a different typical mass of the system. While primordial passive galaxies are related to systems with masses typical of groups at $z > 2.5$, quenched galaxies appear to be a universal phenomenon in clusters, i.e., systems with masses $M_{\rm sys} > 10^{14}\ M_{\odot}$.

We also note that the galaxy mass and luminosity distributions of primordial passive galaxies and quenched galaxies are expected to differ. Since the star formation activity in galaxies proceeds in a downsizing fashion, in both clusters and the field (Cowie et al. 1996; Smail et al. 1998; Kodama & Bower 2001; Poggianti et al. 2001, 2004; Gavazzi et al. 2002; Kauffmann et al. 2003; De Lucia et al. 2004), galaxies terminating their star formation at higher redshift (e.g., primordial passive galaxies) will be on average more massive/luminous than galaxies with a more protracted star formation activity that are quenched at later epochs when they are accreted in the dense environment. As a consequence, quenched galaxies will be on average less massive/fainter than primordial passive galaxies.

Our results show that galaxy properties could be directly linked with the growth history of dark matter structure: as shown in Figures 15 and 16, the history of the mass of structures is reflected in the star-forming fraction we observe. This suggests that, even without using galaxy formation and evolution models, we can use our knowledge of the growth of structure to explain the trends of galaxy properties in clusters. We have only used two pieces of information, namely, how much mass/how many galaxies in a system of a given mass at a given redshift were in dense regions at $z > 2.5$, and how much mass/how many galaxies experienced the cluster environment for at least a few billion years. If this extremely simple, double-channel picture is generally correct, it represents a very powerful recipe for interpreting the environmental trends observed.

If this scenario approximates the real situation, it can also serve as a key to understanding the evolution of galaxy morphologies. We have seen that the observed environmental trends of galaxy properties originate in two ways. The proportion of primordial passive galaxies tends to increase with system mass in high-z systems. Systems with proportionally more massive seeds at $z > 2.5$ formed more primordial passive galaxies (mostly elliptical galaxies). In massive systems, other galaxies are added (as S0 galaxies) to the passive population as time goes by. These are galaxies that would have continued forming stars had they not been acquired by the dense environment that has switched off their star formation activity. From a morphological point of view, it is reasonable to associate the elliptical galaxies with the primordial component and some of the S0 galaxies with the component quenched at $z < 1$.[35] The fact that in some low-z clusters elliptical galaxies have been found to have only old stellar populations, while a significant fraction of the S0 galaxies show signs of a more recent star formation activity, is consistent with this scenario (Kuntschner & Davies 1998; Poggianti et al. 2001; Smail et al. 2001; Terlevich et al. 2001; Thomas 2002). This would also explain why some local clusters are dominated by S0 galaxies and some others by elliptical galaxies. Oemler (1974) suggested that elliptical-rich and S0-rich clusters are not two evolutionary stages in cluster evolution, but intrinsically different types of clusters in which the abundance of elliptical galaxies was established at high redshifts. This suggestion was supported by the findings of Fasano et al. (2000) that clusters at $z \sim 0.1-0.2$ have a low (high) S0/E number ratio if they display (lack) a

[35] As discussed in many previous studies, probably not all S0 galaxies originate from the quenching of spiral galaxies at $z < 1$ (e.g., Dressler et al. 1997). The 0%–20% of S0 galaxies observed in clusters at $z = 0.4-0.8$ might have originated from spiral galaxies evolving into S0 galaxies at $z > 1$, or by some other mechanism. The existence of S0 galaxies in groups (e.g., Hickson et al. 1989) shows that this type of galaxy can be produced also in systems less massive than 400–500 km s^{-1}.

strong concentration of elliptical galaxies toward the cluster center. In the scenario we outline above, elliptical-rich clusters would be those with the highest incidence of primordial passive galaxies, and S0-rich clusters those in which quenched galaxies represent a dominant portion of the passive population.

Let us compare spectroscopic and morphological evolution in more detail. The average fraction of elliptical galaxies in clusters at $z = 0$ from Dressler (1980) is $\sim$20% (see Fasano et al. 2000; V. Desai et al. 2006, in preparation). In agreement with this, at $z = 0$ the fraction of galaxies in halos with masses $>3 \times 10^{12}\ M_{\odot}$ at $z > 2.5$ is $\sim$20% for the majority of systems with $\sigma > 300$ km s^{-1} (Fig. 16, *left panel*). In total, the early-type population (elliptical+S0 galaxies) reaches $\sim$80% at $z = 0$, in agreement with the fraction of passive (non–star-forming) galaxies observed at $z = 0$ (Fig. 4, *right panel*) and with the fraction of passive galaxies (primordial+quenched) of halos at $z = 0$ that were in halos $>10^{14}\ M_{\odot}$ since $z = 0.28$. The observed late-type fraction at all redshifts is in rough agreement with both the observed fraction of star-forming galaxies and the predicted fraction of galaxies that were not in groups at $z = 2.5$ and did not reside in a cluster for at least a few billion years. All of these three quantities are roughly equal to $\sim$20% in clusters at $z = 0$ (compare V. Desai et al. 2006, in preparation, the right panel of Fig. 4, and Fig. 16). All of these three quantities also show a trend with σ at high z (compare V. Desai et al. 2006, in preparation, the left panel of Fig. 4, and Fig. 15).

There is, however, one inconsistency when grossly identifying the population of late-type galaxies with the population of star-forming galaxies. While there is no clear trend in the star-forming fraction with σ at $z = 0$ above 500 km s^{-1} (Fig. 4), the percentage of spiral galaxies in nearby clusters has been shown to anticorrelate with the X-ray luminosity in clusters of $\sigma \sim 700-1000$ km s^{-1} (Bahcall 1977; Edge & Stewart 1991). Although the available morphological studies in X-ray clusters at $z = 0$ were not done in a similar way to ours (for selection of members, radial coverage, morphological classifications, etc.) and notwithstanding the fact that passive spiral galaxies could play an even more important role at low than at high z according to the quenching scenario, this remains an unsolved issue.

Interestingly, significant morphological evolution seems to have taken place in clusters for a large number of galaxies only at $z \leq 0.4$. In fact, as discussed by V. Desai et al. (2006, in preparation), the S0 and spiral galaxy fractions appear to flatten out at $z > 0.45$. A tentative explanation for this behavior can be found in the scenario proposed. At redshifts higher than $\sim$0.6, the population of passive galaxies is generally dominated by primordial passive galaxies (mostly elliptical galaxies, but also the few S0 galaxies present at high redshift). This is supported by the fact that in clusters at redshifts $z \sim 0.6$ (and even more so at $z = 0.8$) the passive fraction can largely be accounted for by the fraction of galaxies that were in dense environments at $z > 2.5$. Only at $z < 0.6$ does the quenched galaxy population become a dominant part of the passive population. Given the delay between the truncation of the star formation and the morphological evolution (Poggianti et al. 1999), this might translate into a morphological evolution observable for a large number of galaxies only at $z < 0.4$.[36] Thus, the epoch where we can observe the quenching of star formation for a significant fraction of galaxies in clusters is only at $z \leq 0.8$, while the epoch where morphological transformations have taken place for a significant fraction of the cluster galaxies is only at $z \leq 0.4$. The redshift range in which these transformations are observable is due to how the relative infall rate (fraction of system mass/galaxies) from low-mass/low-density regions onto clusters/groups changes with redshift, as shown in Figures 15 and 16. Interestingly, $z \sim 0.6$ seems to be a special epoch also for the evolution of quasars in rich environments (Yee & Ellingson 1993).

So far, we have considered the existence of a trend of the O II fraction with σ as a sign of a relation between the star formation of galaxies and the "global environment" (mass of the system) in which galaxies reside. However, it is possible that this is a secondary relation induced by the fact that mass and density are closely linked. In fact, density at early and later times might be the driving factor.

The main galaxy properties (star formation activity and morphology) are observed to vary with the "local" environment in a systematic way. The most emblematic way to describe these systematic variations is the morphology-density (MD) relation, that is, the observed correlation between the frequency of the various Hubble types and the local galaxy density, normally defined as the projected number density of galaxies within an area including its closest 10 neighbors. In clusters in the local universe, the existence of this relation has been known for a long time: elliptical galaxies are frequent in high-density regions, while the fraction of spiral galaxies is high in low-density regions (Oemler 1974; Dressler 1980). An MD relation qualitatively similar to the one observed in the local universe has been observed up to $z = 1$ (as it is logical to expect, galaxy properties correlate with environment at all redshifts), but this relation is quantitatively strongly evolving between $z = 0$ and 0.5: in distant clusters the frequency of S0 galaxies is lower, and the frequency of spiral galaxies higher, at all densities (Dressler et al. 1997). Interestingly, first results at $z = 0.7-1.3$ seem to indicate that between $z = 0.5$ and 1 what changes in the MD relation is only the occurrence of early-type galaxies in the very highest density regions (Smith et al. 2005) and that the frequency of elliptical galaxies at any given local density is the same at $z = 1$ and 0 (Postman et al. 2005).

In parallel to the MD relation, there is a star formation–density (SFD) relation. For a very long time it has been known that in the nearby universe also the average star formation activity correlates with the local density: in higher density regions, the mean star formation rate per galaxy is lower. This is not surprising, given the existence of the MD relation: the highest density regions have proportionally more early-type galaxies devoid of current star formation. The correlation between mean star formation and local density extends to very low local densities, comparable to those found at the virial radius of clusters, and such a correlation exists also outside of clusters (e.g., Lewis et al. 2002; Gomez et al. 2003; Kauffmann et al. 2004). Again, this seems to parallel the fact that an MD relation is probably existing in all environments, and it has been observed in clusters of all types (Dressler 1980), groups (Postman & Geller 1984), and cluster outskirts (Treu et al. 2003), although the MD relation is not quantitatively the same in all environments, being different in concentrated versus irregular clusters and high- versus low-L_X clusters (Dressler 1980; Balogh et al. 2002).

Rephrasing our picture in terms of density instead of mass, both the MD and SFD relations should have a "primordial" component and an "evolved" component, and both of these components should depend on the environment, but in a different way. In this scenario, the MD relation and the SFD relation are

[36] Passive spiral galaxies may be galaxies that are caught in the transition phase of this transformation. Moreover, this might also explain why the morphology-density relation does not evolve much (except in the very highest density bin) between $z = 0.5$ and 1 (Smith et al. 2005); see below. At $z = 1$, the MD (and SFD) relation observed is mostly the primordial relation as established at very high redshift.

established at very high redshift at the moment the first stars formed in galaxies, and they exist due to the close link between the initial star formation activity of galaxies and the primordial local density of their environment (elliptical galaxies formed and have always resided in the highest density regions of the universe). Thus, it could be the "primordial local density" at very high redshift that determines the properties (star formation history, morphology, and probably mass; see Steidel et al. 2005) of galaxies formed in that region. Primordial local density and primordial mass of the cluster seed are probably closely related, and the relation we observe with the fraction of mass in massive environments at $z > 2.5$ could reflect a relation between the primordial local density and the type of galaxy formed in that region.[37] Therefore, the origin of the MD and SFD relations should be "primordial," in the sense that a relation between galaxy properties and environment must have been in place at $z > 3$. In fact, a morphological and star formation segregation is an outcome of cold dark matter (CDM) simulations of large-scale structure and semianalytic models because the local density of galaxies and dark matter is related to the epoch of initial collapse (Bower 1991; Kauffmann 1995a, 1995b; Kauffmann et al. 1999; Benson et al. 2001; Diaferio et al. 2001; Springel et al. 2001): the most massive structures at any epoch are the earliest to collapse. A morphological segregation is built in at a very fundamental level in hierarchical theories of galaxy formation.

However, in addition to this, the MD and SFD relations *evolve* with redshift in a way that depends on environment. In those environments that are effective in quenching star formation, galaxies coming from lower mass/density environments are transformed by environmental effects when they enter the denser region. In fact, all models so far have failed to reproduce the S0 population (which, it is worth remembering, represents >40% of the galaxies in some rich clusters at $z = 0$), recognizing that additional processes seem to be required (Diaferio et al. 2001; Springel et al. 2001; Okamoto & Nagashima 2001, 2003; A. J. Benson et al. 2006, in preparation).

Unfortunately, "trends with environment" have often been confused with "environmental effects," where the latter is used as a synonym for a physical mechanism switching off star formation in infalling galaxies. Thus, for example, the fact that star formation trends exist down to very low local densities and outside of clusters has often been interpreted in the sense that also such low-density environments must somehow "suppress" star formation in galaxies. This is not necessarily the case, as discussed at length above. A trend with environment could be "imprinted" very early on simply due, for example, to the number of galaxies with a short star formation timescale that were able to form at high redshift in that region. To fully comprehend why galaxy properties depend on environment in the way it is observed, it is necessary to disentangle high-z "imprinting" of the initial conditions from "proper" environmental effects acting on galaxies when they experience a dense environment for the first time. The dependence of galaxy properties on environment does not necessarily arise from a "suppression" of star formation: depending on the density/mass of the environment, the relative importance of primordial and quenched passive galaxies can vary significantly.

Two main challenges remain at this point. Observationally, the physical mechanism responsible for quenching the star formation still needs to be identified. The characteristic mass of $M_{\rm sys} > 10^{14}\ M_{\odot}$ (500 km s^{-1}) suggested by this work may help in discriminating among the various processes but still does not uniquely pick out a culprit. Our knowledge of how the efficiency of the various physical mechanisms proposed (e.g., harassment, ram pressure, strangulation) depends on the mass of the system is still too poor to draw solid conclusions and discriminate between them. From a theoretical point of view, one of the most useful pieces of information that can come from state-of-the-art simulations is the link between mass and density at primordial and successive times, as well as the relation between the density experienced by a galaxy at different epochs, to assess whether the relations observed with mass are simply the mirror of relations with density.

[37] Outliers in the O II–mass(σ) relation (groups with low O II fraction and low masses) could be systems with high primordial local density that have grown in mass much less than the average system with similar primordial density.

7. SUMMARY

In this paper we have studied the fraction of galaxies with ongoing star formation as a function of environment at $z = 0.4-0.8$, comparing the results with those at $z = 0$. As a signature for the presence of ongoing star formation, we have used the O II line in emission with an equivalent width stronger than 3 Å.

Our data set is based on 16 high-z clusters with a velocity dispersion $\sigma > 400$ km s^{-1}, 10 groups with 160 km s^{-1} $< \sigma <$ 400 km s^{-1}, and another 250 galaxies in poorer groups and the field with high-quality spectroscopy from the ESO Distant Cluster Survey, plus nine massive clusters at the same redshifts from previous spectroscopic surveys. As a local comparison, we have selected samples of structures from the SDSS at $0.04 < z < 0.08$.

We have presented how the fraction of star-forming galaxies, measured within R_{200}, depends on the velocity dispersion of the cluster/group, at both high and low redshift. We have discussed how the evolution of the fraction of star-forming galaxies compares with the evolution of galaxy morphologies found by previous authors and by our own survey. We propose a simple scenario that is able to account for the origin and the evolution of the observed trends.

In more detail, our results can be summarized as follows:

1. At $z = 0.4-0.8$, most systems follow a broad anticorrelation with significant scatter between the fraction of star-forming galaxies and velocity dispersion: generally, more massive clusters have a lower fraction of star-forming galaxies. This [O II]–σ relation suggests that the mass of the system, although with a significant scatter, largely determines what proportion of galaxies are forming stars at these redshifts.

2. The most evident feature in the O II fraction versus σ diagram observed at high redshift is the presence of a "ridge," or upper envelope, delimiting a region of the diagram where no data point is found. This envelope implies that a system of a given mass at this redshift has *at most* a certain fraction of star-forming galaxies or, equivalently, has *at least* a given fraction of galaxies that are already passive at this epoch. More massive systems have a lower maximum-allowed fraction of star-forming galaxies or, equivalently, a higher minimum-allowed fraction of passive galaxies.

3. We find that at $z = 0.4-0.8$ the field and the poor groups in our sample contain a high proportion of star-forming galaxies (70%–100%) comparable to that observed in more than half of the systems with $\sigma < 400$ km s^{-1}. There are, however, groups with significantly lower O II fractions (<50%). These are outliers that do not follow the [O II]–σ trend defined by the majority of clusters at $z = 0.4-0.8$ and that stand out also for other properties of their galaxies, resembling those of galaxies in the core of

much more massive clusters. The existence and characteristics of the outliers, as well as the fact that the two systems close to other structures possess a low O II fraction for their velocity dispersion, suggest that the factor driving the observed trends might be density, instead of mass. The behavior of the O II fraction with σ might be a secondary relation induced by the fact that mass and density are closely linked.

4. In addition to the fraction of star-forming galaxies, also the star formation properties in star-forming galaxies vary systematically with environment. Environments with higher O II fractions have on average stronger values of equivalent widths of O II among star-forming galaxies. This is due to the fact that both the equivalent width strengths at a given luminosity and the luminosity distribution of star-forming galaxies vary with environment.

5. SDSS clusters at $z = 0.04-0.08$, analyzed in the same way as EDisCS, show significantly lower fractions of star-forming galaxies than clusters at $z \sim 0.4-0.8$. Moreover, SDSS clusters show the existence of a plateau for σ-values above a critical velocity dispersion, equal to $\sim$550 km s^{-1}, above which the O II fraction does not vary systematically with velocity dispersion and remains below 30% for most clusters. A trend still might be present at lower σ-values, with the average O II fraction rising toward lower velocity dispersions.

6. Using N-body simulations to quantify how the mass and velocity dispersion of a cluster or group evolve on average between $z = 0.6$ and 0, we infer the evolutionary connection between systems at $z = 0$ and their progenitors at $z = 0.6$ and quantify the average evolution of the star-forming fraction as a function of velocity dispersion. While the strongest evolution in mass is expected for the most massive structures, the observed evolution of the star-forming fraction is strongest in intermediate-mass systems, those with $\sigma = 500-600$ km s^{-1} at $z = 0$. The evolution is lower in higher and lower mass systems but is still significant even for the most massive systems at $z = 0$. The change in star-forming fractions between $z = 0.4-0.8$ and 0 ranges between 20%–30% and 50%.

7. We compare the proportions of star-forming galaxies with the incidence of late Hubble types (spiral and irregular galaxies). Although in our sample, as in others, star formation activity and morphologies are partly decoupled, we find good agreement between the morphological evolution and the evolution in the star-forming fraction, consistent with the hypothesis that the evolution observed between $z \sim 0.6$ and 0 mostly concerns late-type star-forming galaxies evolving into passive S0 galaxies.

8. Our results quantify the evolution of the star-forming galaxy populations in clusters and groups, for the first time as a function of the mass of the system. Therefore, they are a quantitative description of the Butcher-Oemler effect in its most general sense. The way data points are distributed in the O II fraction versus velocity dispersion at high and low z provides a likely explanation of why it has been so difficult to observe trends with cluster mass/σ and sometimes even with redshift. Only when sampling a very wide range of system masses with large cluster+group samples do the trends become recognizable.

9. To understand the origin of the observed trends between galaxy properties and mass of the environment, we use the Press-Schechter formalism and the Millenium Simulation to investigate whether galaxy star formation histories are related to the growth history of the structures where galaxies reside and have resided during their evolution. We consider a scenario in which the population of passive galaxies (those devoid of ongoing star formation at the time they are observed) consists of two different components: primordial passive galaxies, whose stars all formed at $z > 2.5$, and quenched galaxies, whose star formation has been truncated due to the dense environment at later times. We find that the observed trend of the fraction of passive galaxies with velocity dispersion at $z = 0.4-0.8$ follows the fraction (in mass and in number of galaxies) that is expected to have been in groups ($M_{\rm sys} > 3 \times 10^{12}\ M_{\odot}$) already at $z = 2.5$ and that we identify with the primordial passive population, although in the most massive systems quenched galaxies should already represent a nonnegligible fraction of the passive population. At $z = 0$, on the other hand, the observed fraction of passive galaxies in clusters (80%) resembles the fraction (in mass and in number of galaxies) that has resided in clusters ($M_{\rm sys} > 10^{14}\ M_{\odot}$) during at least the last 3 Gyr, including 20% of primordial passive galaxies and 60% of quenched galaxies. This scheme is able to interpret the observed relations between O II and σ, thus providing a viable quantitative explanation for the evolution of the star formation activity in dense environments and a possible explanation for the origin of the Butcher-Oemler effect. If this scenario approximates the real situation, galaxy star formation histories are closely linked with the galaxy "environmental history," and this link is actually extremely simple to predict.

10. The behavior of the O II fraction with σ at $z = 0$ appears to rule out the hypothesis that the group environment efficiently and universally quenches star formation. In fact, the existence of a plateau in the O II fraction for $\sigma > 500-550$ km s^{-1} at $z = 0$ suggests that only systems more massive than about 450–500 km s^{-1} are highly efficient at truncating star formation in galaxies infalling into them. If the quenching of star formation was a widespread phenomenon also in less massive systems, the fractions of star-forming galaxies in clusters and groups at low redshift should be much lower than is observed. Conversely, the observed reference mass indicates that the quenching of star formation is not limited to very massive clusters but is efficient also in clusters of modest mass.

11. There are numerous implications stemming from the evolutionary scenario proposed. The parallelism between the observed evolution of the star-forming fraction and the morphological evolution suggests that the same physical interpretation of a link with the mass of the environment at $z > 2.5$ and with the accretion history on a cluster can be applied to the formation of elliptical galaxies and at least some of the S0 galaxies, respectively. In fact, the scenario we propose can be used as an interpretative tool for the variations of galaxy properties with environment in general. Our results highlight the fact that not all trends with environment are necessarily linked with environmental processes truncating star formation in recently accreted galaxies and that primordial conditions (i.e., the environment at very high redshift) are an important factor in determining the trends observed with environment. Related to this, we have discussed the consequences of our results for the origin and evolution of the morphology-density and star formation–density relations.

We warmly thank Jarle Brinchmann for helping us use the SDSS products and throughout this project, Risa Wechsler, Frank van den Bosch, and Ray Carlberg for their valuable theoretical advice, Ian Smail for his comments that helped us strengthen an early version of this paper, and the referee, David Wilman, for his careful and detailed report that led to several improvements. We acknowledge the usefulness of the Web sites

maintained by James Bullock and Pieter van Dokkum at http://www.physics.uci.edu/~bullock/CVIR and http://www.astro.yale.edu/dokkum/evocalc (astro-ph/0501236; van Dokkum & Franx 2001), respectively. B. M. P. acknowledges financial support from the "Fondo per gli Investimenti nella Ricerca di Base" of the Italian Ministry of Education, University, and Research (code RBAU018Y7E). G. D. L. thanks the Alexander von Humboldt Foundation, the Federal Ministry of Education and Research, and the Programme for Investment in the Future (ZIP) of the German Government for financial support.

APPENDIX A

SPECTROSCOPIC COMPLETENESS

Here we describe our method for correcting the EDisCS and SDSS spectroscopic samples for incompleteness.

During the EDisCS spectroscopic runs, slits were assigned to galaxies giving preference, whenever possible, to the brightest targets. The SDSS spectroscopic sample was aimed to be complete down to $r = 17.7$, but about 6% of the galaxies were missed due to fiber collision (Strauss et al. 2002), an effect that is likely to be more relevant in crowded regions such as cluster cores. Therefore, it is necessary to quantify how the completeness of the spectroscopic samples varies as a function of galaxy apparent magnitude and of distance from the cluster center.

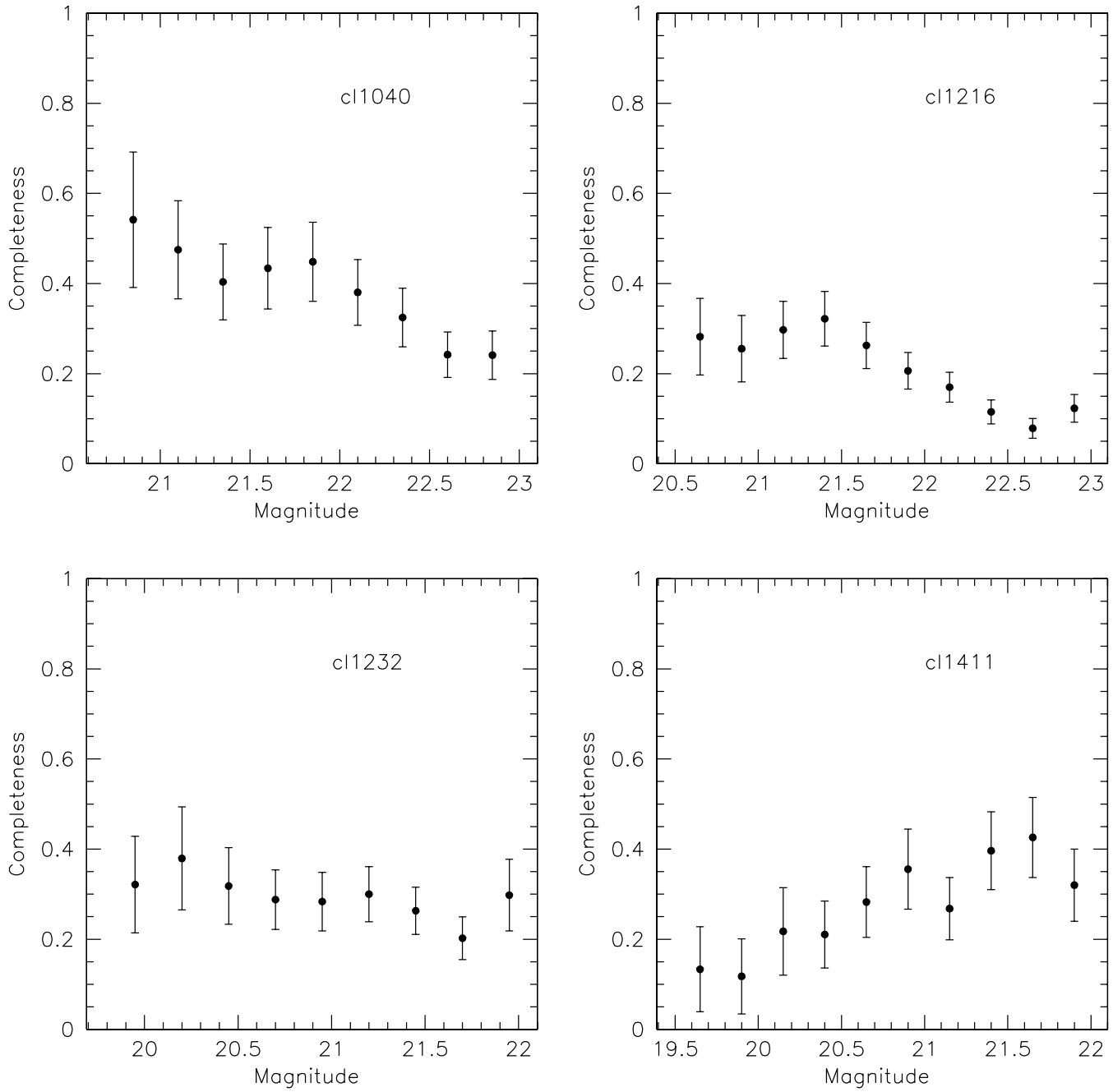

FIG. 17.—Completeness functions vs. galaxy magnitudes for four EDisCS clusters.

TABLE 6
K-S Test Probabilities for the Color Distributions of Spectroscopic and Photometric Catalogs of EDisCS Fields To Be Indistinguishable

Cluster	$p_{\rm cor}^{\rm K\text{-}S}$	$p_{\rm uncor}^{\rm K\text{-}S}$
Cl 1018	0.368	0.250
Cl 1037	0.846	0.996
Cl 1040	0.845	0.845
Cl 1054−11	0.364	0.363
Cl 1054−12	0.246	0.158
Cl 1059	0.371	0.251
Cl 1103	0.515	0.515
Cl 1119	0.251	0.164
Cl 1138	1.000	1.000
Cl 1202	0.018	0.058
Cl 1216	0.245	0.245
Cl 1227	0.686	0.685
Cl 1232	0.249	0.162
Cl 1301	0.685	0.515
Cl 1353	0.249	0.250
Cl 1354	0.246	0.247
Cl 1411	0.518	0.368
Cl 1420	0.518	0.250

As a function of galaxy magnitude, this was done for each field comparing the number of objects in the spectroscopic catalog with the number in the parent photometric catalog in bins of I (for EDisCS) or g (for SDSS) magnitude. The parent catalog included all entries in the EDisCS photometric catalog that were retained as targets for spectroscopy (see Halliday et al. 2004). The ratio of these two numbers yielded a weight as a function of galaxy apparent magnitude ($W_{\rm mag}$). We preferred to compute these weights field by field instead of binning all fields together because, depending on cluster richness and number of masks observed, the behavior of the completeness functions can change significantly. As an example, in Figure 17 we show two clusters for which the completeness decreases toward fainter magnitudes (Cl 1040 and Cl 1216), a cluster where the variations are negligible (Cl 1232), and one of the only two cases in which the completeness increases toward fainter magnitudes (Cl 1411).

We also quantified the presence of eventual geometrical effects due to possible variations in the sampling as a function of the clustercentric radius. Geometrical effects can in principle affect a spectroscopic sample of a cluster due to the fact that cluster galaxies are indeed more "clustered" toward the cluster center while observational constraints on the minimum distance between slits or fibers could result in a lower sampling of these central regions. This effect is expected to be small when several masks of the same cluster, always centered on the cluster center, were taken, as it was the case for EDisCS. Nevertheless, a geometrical completeness $W_{\rm geo}$ was computed, after applying the magnitude completeness correction, comparing the number of galaxies in the spectroscopic and in the parent photometric catalogs in four annuli with $R < 1.4$, $\frac{1}{4} < R < \frac{1}{2}$, $\frac{1}{2} < R < 1$, and $R > 1$ in units of R_{200}. The geometrical corrections hence include corrections for the areas not covered by our FORS2 spectroscopy in the few clusters with incomplete radial sampling out to R_{200}.

The magnitude and geometrical completeness functions, computed cluster by cluster, were applied to the EDisCS and SDSS spectroscopic samples to weight each galaxy accordingly before calculating the O II fractions and the EW(O II) distributions described above. We found that these weights do not alter significantly the O II fractions, as evident from Tables 1 and 3, listing the fractions computed with and without completeness corrections.

APPENDIX B

COLOR SANITY CHECK

As a final check that the EDisCS spectroscopic sample is not biased in any way that depends on the star formation properties of the galaxies, we have compared the color distributions ($B - I$ and $V - I$ for the mid- and high-z samples, respectively) of the spectroscopic sample (with and without completeness corrections) with the color distribution of the parent photometric sample. This has been done field by field, and the resulting K-S test probabilities are given in Table 6. A small probability (<5%) indicates that the two distributions are significantly different and hence that a color bias might be present. The table illustrates a number of results:

1. For all fields except Cl 1202 probabilities are high even when the spectroscopy has not been corrected for completeness (col. [3]). Evidently, even the uncorrected samples do not show a strong color bias. In principle, this was not guaranteed a priori because, although targets for spectroscopy were drawn from the parent targeting catalog with no color criterion, slits were preferentially assigned to the brightest galaxies first, and this could have introduced a difference in the color distribution of the two samples.

2. For eight fields the probabilities increase (therefore the agreement between the two color distributions improves) once the completeness corrections are taken into account. This indicates that indeed the corrections yield a sample even more closely representative of the whole galaxy distributions. For another eight clusters, the probabilities remain unchanged with and without completeness corrections.

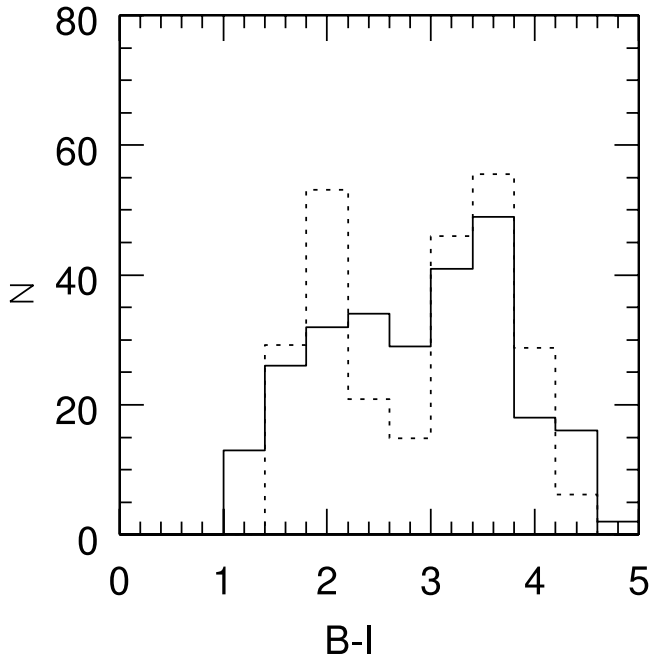

FIG. 18.—Color distributions of the parent photometric catalog (*solid histogram*) and of the spectroscopic catalog corrected for incompleteness (*dashed histogram*) for the cluster Cl 1202.

3. Two fields behave differently from the above. When including completeness corrections, the probability for Cl 1037 slightly decreases, although it remains high (0.85), ruling out a color bias. Cl 1202 is the cluster with the lowest probabilities (0.058 and 0.018 without and with corrections, respectively). The color distributions for Cl 1202 are shown in Figure 18. The plot shows that there is no strong bias toward either red or blue galaxies; therefore, we do not expect the O II fraction derived for this cluster to be strongly biased.

Figure 19 compares the color distributions of the spectroscopic catalogs and the parent photometric catalogs for all clusters, grouping together the mid-z clusters (with B photometry; *left panel*) and the high-z clusters (V photometry; *right panel*). As Table 6, also the figure illustrates that no significant color bias is present in our spectroscopic sample. We conclude that the O II fractions derived in this paper are representative within the errors of the "true" fractions in the EDisCS clusters to the adopted magnitude limits.

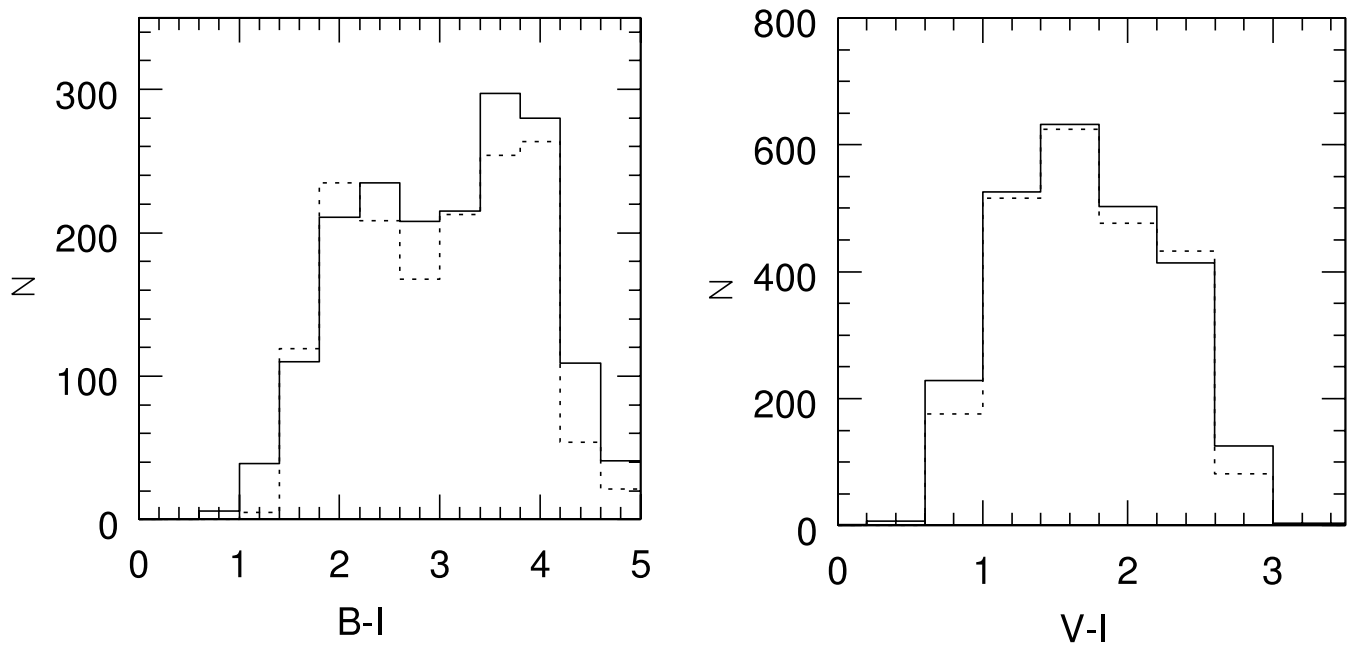

FIG. 19.—*Left*: Color distribution of the parent photometric catalog (*solid histogram*) and the spectroscopic catalog corrected for completeness (*dashed histogram*) for the nine clusters with B photometry. *Right*: Same as left panel, but for clusters with V photometry.

APPENDIX C

VELOCITY DISPERSION OF SDSS CLUSTERS

As for the EDisCS sample, we rely on the biweight estimator of Beers et al. (1990) for determining the cluster redshift z_C and velocity dispersion σ_v of SDSS clusters:

1. To begin with, we chose galaxies within 2.2 Abell radii of the BCG and within ± 0.015 from the cluster redshift as given by Struble & Rood (1991). From these galaxies, first estimates of the cluster redshift z_C and the velocity dispersion σ_z were calculated as the median and the median absolute deviation. If σ_z was larger than 0.0017 (corresponding to about 500 km s^{-1} at $z = 0$), we set it to this value. This step was necessary to avoid too much contamination from surrounding structures.
2. From those galaxies within $\pm 3\sigma_z$ from z_C and $1.2R_{200}$ (calculated from z and σ_z using eq. [1]), we recalculated first z and then σ_z via the biweight estimators given in Beers et al. (1990).
3. This process was iterated until it reached convergence. At each round, every galaxy in the initial sample can reenter the cluster sample if it meets the constraints on redshift and velocity.
4. The error on the final σ_z is calculated from a bootstrap analysis of the galaxies that make up the final cluster sample.

REFERENCES

Allington-Smith, J. R., Ellis, R., Zirbel, E. L., & Oemler, A., Jr. 1993, ApJ, 404, 521
Andreon, S., & Ettori, S. 1999, ApJ, 516, 647
Bahcall, N. A. 1977, ApJ, 218, L93
Balogh, M. L., Bower, R. G., Smail, I., Ziegler, B. L., Davies, R. L., Gaztelu, A., & Fritz, A. 2002, MNRAS, 337, 256
Balogh, M. L., Morris, S. L., Yee, H. K. C., Carlberg, R. G., & Ellingson, E. 1997, ApJ, 488, L75
Balogh, M. L., Schade, D., Morris, S. L., Yee, H. K. C., Carlberg, R. G., & Ellingson, E. 1998, ApJ, 504, L75
Balogh, M. L., et al. 2004, MNRAS, 348, 1355
Bamford, S. P., Milvang-Jensen, B., Aragón-Salamanca, A., & Simard, L. 2005, MNRAS, 361, 109
Barger, A. J., et al. 1998, ApJ, 501, 522
Barrientos, L. F., Gladders, M. D., Yee, H. K. C., Infante, L., Ellingson, E., Hall, P. B., & Hertling, G. 2004, ApJ, 617, L17
Beers, T. C., Flynn, K., & Gebhardt, K. 1990, AJ, 100, 32
Benson, A. J., Frenk, C. S., Baugh, C. M., Cole, S., & Lacey, C. G. 2001, MNRAS, 327, 1041
Biviano, A., Katgert, P., Mazure, A., Moles, M., den Hartog, R., Perea, J., & Focardi, P. 1997, A&A, 321, 84
Blakeslee, J. P., et al. 2003, ApJ, 596, L143
Bower, R. 1991, MNRAS, 248, 332
Bower, R. G., Lucey, J. R., & Ellis, R. S. 1992, MNRAS, 254, 601
Brinchmann, J., Charlot, S., Heckman, T. M., Kauffmann, G., Tremonti, C., & White, S. D. M. 2004a, preprint (astro-ph/0406220)
Brinchmann, J., Charlot, S., White, S. D. M., Tremonti, C., Kauffmann, G., Heckman, T., & Brinkmann, J. 2004b, MNRAS, 351, 1151
Bullock, J. S., Kolatt, T. S., Sigad, Y., Somerville, R. S., Kravtsov, A. V., Klypin, A. A., Primack, J. R., & Dekel, A. 2001, MNRAS, 321, 559
Butcher, H., & Oemler, A., Jr. 1978, ApJ, 226, 559
———. 1984, ApJ, 285, 426
Cid Fernandes, R., Gu, Q., Melnich, J., Terlevich, E., Terlevich, R., Kunth, D., Rodriguess Lacerda, R., & Joguet, B. 2004, MNRAS, 355, 273
Clowe, D. I., et al. 2006, A&A, in press (astro-ph/0511746)
Couch, W. J., Balogh, M. L., Bower, R. G., Smail, I., Glazebrook, K., & Taylor, M. 2001, ApJ, 549, 820
Couch, W. J., Barger, A. J., Smail, I., Ellis, R. S., & Sharples, R. M. 1998, ApJ, 497, 188
Couch, W. J., & Sharples, R. M. 1987, MNRAS, 229, 423
Cowie, L. L., Songaila, A., Hu, E. M., & Cohen, J. G. 1996, AJ, 112, 839
Croton, D. J., et al. 2006, MNRAS, 365, 11 (erratum 367, 864)
De Lucia, G., Springel, V., White, S. D. M., Croton, D., & Kauffmann, G. 2006, MNRAS, 366, 499
De Lucia, G., et al. 2004, ApJ, 610, L77
Demarco, R., et al. 2005, A&A, 432, 381
De Propris, R., et al. 2004, MNRAS, 351, 125
Diaferio, A., Kauffmann, G., Balogh, M., White, S. D. M., Schade, D., & Ellingson, E. 2001, MNRAS, 323, 999
Dressler, A. 1980, ApJ, 236, 351
Dressler, A., & Gunn, J. E. 1982, ApJ, 263, 533
———. 1983, ApJ, 270, 7
———. 1992, ApJS, 78, 1
Dressler, A., Oemler, A., Jr., Poggianti, B. M., Smail, I., Trager, S., Shectman, S. A., Couch, W. J., & Ellis, R. S. 2004, ApJ, 617, 867
Dressler, A., Smail, I., Poggianti, B. M., Butcher, H., Couch, W. J., Ellis, R. S., & Oemler, A., Jr. 1999, ApJS, 122, 51
Dressler, A., et al. 1997, ApJ, 490, 577
Edge, A. C., & Stewart, G. C. 1991, MNRAS, 252, 428
Ellingson, E., Lin, H., Yee, H. K. C., & Carlberg, R. G. 2001, ApJ, 547, 609
Ellis, R. S., Smail, I., Dressler, A., Couch, W. J., Oemler, A., Jr., Butcher, H., & Sharples, R. M. 1997, ApJ, 483, 582
Fairley, B. W., Jones, L. R., Wake, D. A., Collins, C. A., Burke, D. J., Nichol, R. C., & Romer, A. K. 2002, MNRAS, 330, 755
Fasano, G., Poggianti, B. M., Couch, W. J., Bettoni, D., Kjaergaard, P., & Moles, M. 2000, ApJ, 542, 673
Finn, R. A., Zaritsky, D., & McCarthy, D. W. 2004, ApJ, 604, 141
Finn, R. A., et al. 2005, ApJ, 630, 206
Fisher, D., Fabricant, D., Franx, M., & van Dokkum, P. 1998, ApJ, 498, 195
Gal, R. R., & Lubin, L. M. 2004, ApJ, 607, L1
Gavazzi, G., Boselli, A., Pedotti, P., Gallazzi, A., & Carrasco, L. 2002, A&A, 396, 449
Girardi, M., & Mezzetti, M. 2001, ApJ, 548, 79
Gomez, P. L., et al. 2003, ApJ, 584, 210
Gonzalez, A. H., Zaritsky, D., Dalcanton, J. J., & Nelson, A. 2001, ApJS, 137, 117
Goto, T. 2005, MNRAS, 356, L6
Goto, T., et al. 2003, PASJ, 55, 757
Gray, M. E., Wolf, C., Meisenheimer, K., Taylor, A., Dye, S., Borch, A., & Kleinheinrich, M. 2004, MNRAS, 347, L73
Halliday, C., et al. 2004, A&A, 427, 397
Heckman, T., et al. 1995, ApJ, 452, 549
Hickson, P., Kindl, E., & Auman, J. R. 1989, ApJS, 70, 687
Holden, B. P., et al. 2005, ApJ, 626, 809
Homeier, N. L., et al. 2005, ApJ, 621, 651
Hopkins, A. M. 2004, ApJ, 615, 209
Kauffmann, G. 1995a, MNRAS, 274, 153
———. 1995b, MNRAS, 274, 161
Kauffmann, G., Colberg, J. M., Diaferio, A., & White, S. D. M. 1999, MNRAS, 307, 529
Kauffmann, G., White, S. D. M., Heckman, T. M., Ménard, B., Brinchmann, J., Charlot, S., Tremonti, C., & Brinkmann, J. 2004, MNRAS, 353, 713
Kauffmann, G., et al. 2003, MNRAS, 341, 54
Kewley, L. J., Jansen, R. A., & Geller, M. J. 2005, PASP, 117, 227
Kodama, T., Arimoto, N., Barger, A. J., & Aragón-Salamanca, A. 1998, A&A, 334, 99
Kodama, T., Balogh, M. L., Smail, I., Bower, R. G., & Nakata, F. 2004, MNRAS, 354, 1103
Kodama, T., & Bower, R. G. 2001, MNRAS, 321, 18
Kuntschner, H., & Davies, R. L. 1998, MNRAS, 295, L29
Lacey, C., & Cole, S. 1993, MNRAS, 262, 627
Lewis, I., et al. 2002, MNRAS, 334, 673
Lilly, S. J., Le Fevre, O., Hammer, F., & Crampton, D. 1996, ApJ, 460, L1
Lubin, L. M., Oke, J. B., & Postman, M. 2002, AJ, 124, 1905
Madau, P., Pozzetti, L., & Dickinson, M. 1998, ApJ, 498, 106
Margoniner, V. E., & de Carvalho, R. R. 2000, AJ, 119, 1562
Margoniner, V. E., de Carvalho, R. R., Gal, R. R., & Djorgovski, S. G. 2001, ApJ, 548, L143
Martinez, H. J., Zandivarez, A., Dominguez, M., Merchan, M. E., & Lambas, D. G. 2002, MNRAS, 333, L31
Miller, C. J., et al. 2005, AJ, 130, 968
Milvang-Jensen, B., Aragón-Salamanca, A., Hau, G. K. T., Jorgensen, I., & Hjorth, J. 2003, MNRAS, 339, L1

Moran, S. M., Ellis, R. S., Treu, T., Smail, I., Dressler, A., Coil, A. L., & Smith, G. P. 2005, ApJ, 634, 977
Nakata, F., Bower, R. G., Balogh, M. L., & Wilman, D. J. 2005, MNRAS, 357, 679
Oemler, A., Jr. 1974, ApJ, 194, 1
Okamoto, T., & Nagashima, M. 2001, ApJ, 547, 109
———. 2003, ApJ, 587, 500
Poggianti, B. M., Bridges, T. J., Komiyama, Y., Yagi, M., Carter, D., Mobasher, B., Okamura, S., & Kashikawa, N. 2004, ApJ, 601, 197
Poggianti, B. M., Smail, I., Dressler, A., Couch, W. J., Barger, A. J., Butcher, H., Ellis, R. S., & Oemler, A., Jr. 1999, ApJ, 518, 576
Poggianti, B. M., et al. 2001, ApJ, 562, 689
Postman, M., & Geller, M. J. 1984, ApJ, 281, 95
Postman, M., Lubin, L. M., & Oke, J. B. 1998, AJ, 116, 560
———. 2001, AJ, 122, 1125
Postman, M., et al. 2005, ApJ, 623, 721
Press, W. H., Teukolsky, S. A., Vetterling, W. T., & Flannery, B. P. 1986, Numerical Recipes in FORTRAN 77 (Cambridge: Cambridge Univ. Press)
Rudnick, G., et al. 2003, ApJ, 599, 847
Schiminovich, D., et al. 2005, ApJ, 619, L47
Smail, I., Edge, A. C., Ellis, R. S., & Blandford, R. D. 1998, MNRAS, 293, 124
Smail, I., Kuntschner, H., Kodama, T., Smith, G. P., Packham, C., Fruchter, A. S., & Hook, R. N. 2001, MNRAS, 323, 839
Smith, G. P., Treu, T., Ellis, R. S., Moran, S. M., & Dressler, A. 2005, ApJ, 620, 78
Springel, V., White, S. D. M., Tormen, G., & Kauffmann, G. 2001, MNRAS, 328, 726
Springel, V., et al. 2005, Nature, 435, 629
Steidel, C. C., Adelberger, K. L., Shapley, A. E., Erb, D. K., Reddy, N. A., & Pettini, M. 2005, ApJ, 626, 44
Strauss, M. A., et al. 2002, AJ, 124, 1810
Struble, M. F., & Rood, H. J. 1991, ApJS, 77, 363
Terlevich, A. I., Caldwell, N., & Bower, R. G. 2001, MNRAS, 326, 1547
Thomas, T. 2002, Ph.D. thesis, Leiden Univ.
Tran, K.-V. H., Franx, M., Illingworth, G. D., Kelson, D. D., & van Dokkum, P. 2003, ApJ, 599, 865
Tran, K.-V. H., van Dokkum, P., Illingworth, G. D., Kelson, D., Gonzalez, A., & Franx, M. 2005, ApJ, 619, 134
Treu, T., Ellis, R. S., Kneib, J.-P., Dressler, A., Smail, I., Czoske, O., Oemler, A., & Natarajan, P. 2003, ApJ, 591, 53
Umeda, K., et al. 2004, ApJ, 601, 805
van Dokkum, P. G., & Franx, M. 2001, ApJ, 553, 90
van Dokkum, P. G., Franx, M., Fabricant, D., Illingworth, G. D., & Kelson, D. D. 2000, ApJ, 541, 95
van Dokkum, P. G., Stanford, S. A., Holden, B. P., Eisenhardt, P. R., Dickinson, M., & Elston, R. 2001, ApJ, 552, L101
Wechsler, R. H., Bullock, J. S., Primack, J. R., Kravtsov, A. V., & Dekel, A. 2002, ApJ, 568, 52
Weinmann, S. M., van den Bosch, F. C., Yang, X., & Mo, H. J. 2006, MNRAS, 366, 2
White, S. D. M., et al. 2005, A&A, 444, 365
Wilman, D. J., Balogh, M. L., Bower, R. G., Mulchaey, J. S., Oemler, A., Carlberg, R. G., Morris, S. L., & Whitaker, R. J. 2005a, MNRAS, 358, 71
Wilman, D. J., et al. 2005b, MNRAS, 358, 88
Yee, H. K. C., & Ellingson, E. 1993, ApJ, 411, 43
Zabludoff, A. I., & Mulchaey, J. S. 1998, ApJ, 496, 39